Structural modeling reveals the mechanism of motor ATPase coordination during type IV pilus retraction

Abigail E. Teipen[1], Jacob D. Holt[2,3], Diane L. Lynch[4,5], Yixuan Peng[2,3], Triana N. Dalia[1], James C. Gumbart[4,5,*], Carey D. Nadell[2,3,*], Ankur B. Dalia[1,*]

[1]Department of Biology, Indiana University, Bloomington, IN 47405
[2]Department of Biological Sciences, Dartmouth, Hanover, NH 03755
[3]Department of Microbiology and Immunology, Geisel School of Medicine at Dartmouth, Hanover, NH 03755
[4]School of Physics, Georgia Institute of Technology, Atlanta, Georgia 30332
[5]School of Chemistry & Biochemistry, Georgia Institute of Technology, Atlanta, Georgia 30332

*To whom correspondence may be addressed. Email: ankdalia@iu.edu, carey.d.nadell@dartmouth.edu, and gumbart@physics.gatech.edu

ABSTRACT

Diverse bacterial species utilize surface appendages called type IV pili (T4P) to interact with their environment. These structures are dynamically extended and retracted from the cell surface, which is critical for diverse functions. Some T4P systems rely on two distinct motor ATPases, PilT and PilU, whose combined activities are required to power forceful T4P retraction. However, the mechanism by which these motors coordinate to facilitate T4P retraction has remained unclear. Here, we utilize the competence T4P in *V. cholerae* as a model system to elucidate the molecular basis for PilT-PilU coordination during T4P retraction. Specifically, we modeled the interactions between PilT and PilU using AlphaFold 3 and molecular dynamics (MD) simulations. We then empirically tested these models using a combination of cytological and high-resolution genetic approaches. Our results reveal that interactions between PilT and the PilU C-terminus are critical for these motors to coordinate to drive T4P retraction. Finally, we show that PilT-PilU interactions are broadly conserved in T4P systems from diverse bacterial species, and we experimentally validate that they are required for T4P retraction in *Acinetobacter baylyi*. Together, this work expands our fundamental understanding of T4P dynamics, and more broadly it provides mechanistic insight into how these ATPases coordinate to assemble some of the strongest biological motors in nature.

SIGNIFICANCE

Diverse bacterial species use filamentous surface appendages called type IV pili (T4P) to move along surfaces, take up DNA for horizontal gene transfer, and stick to biotic and abiotic surfaces. The forceful retraction of these filaments is often required for these behaviors. In many T4P systems, the combined activity of two distinct motor ATPase proteins is required for forceful retraction; however, a detailed understanding of *how* these motor proteins interact to promote forceful retraction is currently lacking. Here, we use an integrated approach to uncover the molecular mechanism for motor ATPase coordination. Furthermore, we show that this mechanism is broadly conserved in diverse T4P systems.

INTRODUCTION

Type IV pili (T4P) are broadly conserved proteinaceous surface appendages that mediate several important behaviors including DNA uptake for natural transformation, surface attachment, surface sensing, and twitching motility (1-5). The T4P machine is a large macromolecular complex composed of at least 80 proteins (via a multimeric assembly of 7 unique proteins) (6-8). This nanomachine dynamically assembles (extends) and disassembles (retracts) a pilus fiber through an outer membrane gated secretin (9, 10), and this dynamic extension and retraction is critical for the diverse functions carried out by T4P (2, 4, 11).

In canonical T4P (*i.e.*, type IVa pilus systems), dynamic extension and retraction are powered by distinct hexameric motor ATPases. Pilus extension is often driven by a single motor ATPase protein, PilB, that interacts with the T4P platform protein, PilC, and hydrolyzes ATP to power the assembly of major pilin subunits into a helical pilus filament that extends from the cell surface (12, 13). Conversely, T4P retraction is commonly powered by two distinct motor ATPases – PilT and PilU. Previous studies have established that PilT serves as the primary retraction ATPase (12, 14, 15) that directly interacts with PilC to promote depolymerization of major pilin subunits. PilU is an accessory ATPase (16, 17) that drives forceful T4P retraction in a PilT-dependent manner (18-20). A detailed mechanistic understanding of *why* PilU requires PilT to promote retraction and *how* PilT and PilU coordinate to promote forceful T4P retraction, however, remains unclear.

In this study, we use the *Vibrio cholerae* competence T4P as a model system to dissect the molecular mechanism underlying PilT-PilU-mediated retraction. The *V. cholerae* competence T4P is required for DNA uptake during horizontal gene transfer by natural transformation (NT) (1). During this process, competence T4P extend from the bacterial surface, bind to DNA in the environment, and then retract to bring this DNA into the cell (11, 21). This DNA is then translocated into the cytoplasm and if it is homologous to the host genome, it can be integrated by homologous recombination (22). NT is induced when *V. cholerae* colonizes the chitinous shells of crustacean zooplankton in the aquatic environment (23). Recent work highlights that PilU-dependent retraction is necessary for NT when DNA is adsorbed to a chitin surface (24). Thus, PilT and PilU are both critical for facilitating DNA uptake by competence T4P under physiologically relevant conditions. Also, the *V. cholerae* competence T4P has emerged as an invaluable model system for studying the basic biology of T4P (11, 18, 19, 25-27). Thus, it is ideally suited for dissecting the molecular mechanism underlying PilT-PilU coordination during T4P retraction.

RESULTS

AlphaFold 3 models interactions between the retraction motor ATPases and the T4P machine

To define how PilT and PilU coordinate to facilitate T4P retraction, we first sought to model their interactions with PilC using AlphaFold 3 (AF3) (28). Due to the large size of this complex, we generated a hybrid model of PilC-PilT-PilU by independently modeling the interaction between 1) PilC and the PilT hexamer and 2) the PilT and PilU hexamers (**Fig S1a-b**). Then, one subunit of PilT was aligned between these two models to generate the hybrid complex (**Fig. 1a**).

The relatively high model confidence scores for PilT-PilC (ipTM = 0.66) and PilT-PilU (ipTM = 0.63) suggest that PilT may directly interact with both PilC and PilU (**Fig S1a-b**). By contrast, AF3 modeling of PilU-PilC yields very low confidence models (ipTM = 0.37), which may suggest that PilU and PilC do not directly interact (**Fig S1c**). Because PilT is predicted to interact with PilC and PilU via distinct interfaces (**Fig 1a**), we hypothesize that PilU requires PilT to engage the T4P machine. This model is consistent with prior work demonstrating that PilU can only facilitate T4P retraction in the presence of PilT (18, 19, 26).

PilT bridges PilU to the T4P machine

To test whether PilU requires PilT to engage the T4P machine, we sought to develop an assay to examine the interaction of these ATPases with the T4P machine in live cells. When the ATPase activity of these motors is intact (*pilT*$^{+}$ and/or *pilU*$^{+}$), it is likely that they only engage the T4P machine transiently while actively promoting T4P retraction. Accordingly, strains expressing *mCherry-pilT*$^{+}$ and *mCherry-pilU*$^{+}$ rarely form foci at the cell periphery (**Fig. S2**). We hypothesized that we could stabilize the interaction of these ATPases with the T4P machine by ablating their ATPase activity via mutation of the Walker A (WA) site required for ATP-binding (*pilT*^{WA} = *pilT*^{K136A}; *pilU*^{WA} = *pilU*^{K134A}) (18, 29). Indeed, in strains expressing *mCherry-pilT*^{WA} *pilU*^{WA} and *pilT*^{WA} *mCherry-pilU*^{WA}, stable fluorescent foci are readily observed at the cell periphery in the majority of cells (**Fig. 1b-d**). Importantly, these foci are ablated in a strain lacking the platform proteins of the competence T4P (*pilC*) and MSHA T4P (*mshG*), both of which can be retracted by PilT and PilU (**Fig. 1c-d**) (19, 30, 31). These results suggest that mCherry-PilT^{WA} and mCherry-PilU^{WA} foci represent motor ATPases that are bound to a T4P machine.

The AF3 model suggests that PilT directly interacts with the T4P machine; thus, we hypothesized that PilU would be dispensable for PilT-T4P interactions. Consistent with this, *mCherry-pilT*^{WA} Δ*pilU* cells still readily formed fluorescent foci (**Fig 1c**). Importantly, deletion of the T4P platform proteins still ablates focus formation in this background (**Fig 1c**). By contrast, the AF3 model suggests that PilT is required to bridge the interaction between PilU and the T4P machine (**Fig. 1a**). Indeed, fluorescent foci are ablated in *mCherry-pilU*^{WA} Δ*pilT* compared to the *mCherry-pilU*^{WA} *pilT*^{WA} parent (**Fig. 1d**). Together these results indicate that PilT may directly interact with the T4P machine, and that PilT is required to bridge PilU-T4P interactions.

The AF3 model also predicts a direct interaction between PilT and PilU. Accordingly, in *pilT*^{WA}-*mCherry gfp-pilU*^{WA} cells, 96% ± 2% of the GFP-PilU^{WA} foci overlap with a PilT^{WA}-mCherry focus (**Fig. 1e**). This colocalization is consistent with these ATPase motors interacting at the same T4P machine as suggested by the AF3 model.

Our data thus far strongly suggest that PilT and PilU interact with one another to engage the T4P machine, which is consistent with the AF3 model. This is also supported by a recent preprint that analyzes the *V. cholerae* competence T4P machine *in situ* via cryo-EM. In strains expressing *pilT*^{WA} and *pilU*^{WA}, subtomogram averages revealed the presence of two stacked densities below the T4P machine (32), which is consistent with stacked PilT and PilU hexamers engaging the T4P machine. Altogether, these results support the ultrastructural organization of the PilC-PilT-PilU complex predicted by the AF3 hybrid model.

Interactions between PilT and the PilU$^{C\text{-}term}$ are critical for T4P retraction

Our data thus far suggest that PilT and PilU interact and that this interaction is likely required for PilU to engage the T4P machine. Next, we sought to employ the PilT-PilU AF3 model to further define the molecular basis for motor ATPase coordination.

Competence T4P retraction is necessary for DNA uptake (1, 11); thus, NT serves as a simple, yet sensitive readout (>5-logs of dynamic range) for T4P retraction (**Fig. 2b**). Competence T4P can also be directly imaged in *V. cholerae* via introduction of a cysteine into the major pilin (*pilA^{S67C}*), which allows for subsequent labeling with fluorescent maleimide dyes (11, 33). Strains that are competent for T4P retraction have very few extended pili because competence T4P are highly dynamic (**Fig. 2c**, parent). In contrast, strains that cannot retract competence T4P become hyperpiliated due to the accumulation of static extended pili on the cell surface (**Fig. 2c**, Δ*pilT*). Competence T4P also self-interact (27); thus, hyperpiliated cells form large multi-cellular aggregates that "floc" out of solution (**Fig. 2c**) (18). PilU is normally dispensable for competence T4P retraction, however, if cells contain a PilT^{WA} mutation, retraction becomes dependent on PilU (18, 19), a finding that we recapitulate here (**Fig. 2b-c**, compare Δ*pilU* to *pilT^{WA}* Δ*pilU*). Thus, the *pilT^{WA}* background can be used to assess PilT-PilU-dependent retraction (*i.e.*, retraction that is dependent on <u>both</u> motor ATPases), while a background where PilT ATPase activity is intact and *pilU* is deleted (*pilT^{+}* Δ*pilU*) can be used to assess PilT-dependent retraction (*i.e.*, retraction that is only dependent on PilT). For this reason, we initially focused on mutating the PilT side of the PilT-PilU interface to define regions that are 1) critical for these motors to coordinate and promote PilT-PilU-dependent T4P retraction but 2) dispensable for PilT-dependent retraction.

Analysis of the AF3 model revealed three distinct regions of PilT that putatively form salt bridges with PilU – PilT^{D2,E53}, PilT^{R35,K36}, and PilT^{E64,E65} (**Fig. 2a and Fig. S3**). To test if any of these areas are required for PilT-PilU-dependent retraction, we mutated these PilT residues to alanines and assessed pilus retraction using NT, direct observation of competence T4P, and cellular aggregation as described above. The phenotype of *pilT^{WA,E64A,E65A}* was indistinguishable from *pilT^{WA}*, suggesting that this region is dispensable for PilT-PilU-dependent retraction (**Fig. 2b-c**). By contrast, *pilT^{WA,R35A,K36A}* and *pilT^{WA,D2A,E53A}* resulted in an ~3.5-log decrease in NT (compared to *pilT^{WA}*) and a strong hyperpiliation and aggregation phenotype which is consistent with these two regions playing an important role in PilT-PilU-dependent retraction (**Fig. 2b-c**). Importantly, mutating these three regions (*pilT^{E64A,E65A}*, *pilT^{D2A,E53A}*, and *pilT^{R35A,K36A}*) does not diminish PilT-dependent T4P retraction (*i.e.*, retraction in a *pilT^{+}* Δ*pilU* background), indicating that PilT^{D2,E53} and PilT^{R35,K36} are specifically required for PilT-PilU-dependent retraction (**Fig. 2b-c**).

The reduction in PilT-PilU-dependent retraction observed in *pilT^{D2A,E53A}* and *pilT^{R35A,K36A}* may be due to an effect of these mutations on either (1) diminishing PilT-PilU interactions or (2) preventing PilT-PilU coordination without affecting their interaction. To distinguish between these, we assessed the effect of these mutations on PilT and PilU localization to T4P machines. We hypothesized that if these regions are required for PilT-PilU interactions, mutating these residues in a *pilT^{WA} mCherry-pilU^{WA}* background would result in loss of mCherry-PilU^{WA} foci. When we performed this analysis, *pilT^{WA,D2A,E53A} mCherry-pilU^{WA}* and *pilT^{WA,R35A,K36A} mCherry-*

pilU^{WA} no longer formed mCherry-PilU^{WA} foci (**Fig. 2d**) which is consistent with the loss of T4P retraction observed in these backgrounds (**Fig. 2b-c**). Also, *pilT*^{WA,E64A,E65A} *mCherry-pilU*^{WA} still formed mCherry-PilU^{WA} foci and was indistinguishable from the *pilT*^{WA} *mCherry-pilU*^{WA} parent (**Fig. 2d**), which is consistent with this mutation having no effect on PilT-PilU-dependent retraction (**Fig. 2b-c**). Importantly, mCherry-PilT^{WA,E64A,E65A}, mCherry-PilT^{WA,D2A,E53A}, and mCherry-PilT^{WA,R35A,K36A} all localized to T4P machines just like the mCherry-PilT^{WA} parent (**Fig. 2e**), which is consistent with these mutations having no effect on PilT-dependent retraction (**Fig. 2b-c**). Together, these data suggest that PilT^{D2,E53} and PilT^{R35,K36} are important for the interaction between PilT and PilU that allow this complex to coordinate retraction.

PilT^{D2,E53} and PilT^{R35,K36} are both predicted to interact with the PilU C-terminus (PilU$^{C\text{-term}}$). PilT and PilU are highly homologous motor ATPases, however the extended C-terminal domain is a unique feature of PilU homologs (**Fig. S4**)**.** The AF3 model predicts that the PilU$^{C\text{-term}}$ wraps around the sides of the PilT hexamer (**Fig. 2a**). Because our mutational analysis demonstrates that PilT^{D2,E53} and PilT^{R35,K36} diminish PilT-PilU-dependent retraction (**Fig. 2**), we hypothesized that interactions between PilT and the PilU$^{C\text{-term}}$ are critical for PilT-PilU mediated T4P retraction.

To test this hypothesis at a higher resolution, we targeted the putative intermolecular salt bridges formed between PilT^{D2,E53}-PilU^{K348}, PilT$^{R35\text{-}}$PilU^{D366,E368}, PilT^{K36}-PilU^{D366} for mutagenesis by flipping their charge (**Fig 3a**). We reasoned that flipping the charge on either side of the intermolecular salt bridge should have a repulsive effect that breaks PilT-PilU interactions, which should disrupt pilus retraction. However, flipping the charge on both sides of the salt bridge should repair the interaction and restore T4P retraction. Importantly, restoration of T4P retraction in the double charge-flip mutant should only occur if the two residues interact, thus, providing an easy genetic approach for testing the residue-level accuracy of the PilT-PilU interactions predicted by AF3.

As shown above, mutating the PilT side of the interface allows us to test whether mutations specifically affect PilT-PilU-dependent retraction (tested in the *pilT*^{WA} background) without disrupting PilT-dependent retraction (tested in the *pilT*$^{+}$ Δ*pilU* background). By contrast, mutating the PilU side of the interface cannot distinguish between 1) disruption of the PilT-PilU interface and 2) mutations that cause PilU to misfold. Thus, we first assessed the impact of flipping the charge on the PilT side of the interface in the three predicted salt bridge contacts (*pilT*^{R35E}, *pilT*^{K36E}, and *pilT*^{D2K,E53R}). All three mutants resulted in a decrease in NT, with *pilT*^{R35E} and *pilT*^{D2K,E53R} causing the most severe loss of retraction (**Fig. 3b-c**). Importantly, these mutations had no observable impact on PilT-dependent retraction (**Fig. S5**). Thus, disrupting the PilT side of the putative PilT^{D2,E53}-PilU^{K348}, PilT^{R35}-PilU^{D366,E368}, and PilT^{K36}-PilU^{D366} salt bridges specifically inhibited PilT-PilU-dependent T4P retraction.

To further probe the validity of these intermolecular salt bridges, we sought to flip the charge on the PilU side of the interface to test whether this recovered T4P retraction. The AF3 model indicates that PilT^{R35} makes contacts with both PilU^{D366} and PilU^{E368} (**Fig. S3b**). The *pilT*^{WA,R35E} *pilU*^{D366K,E368K} strain, however, remained hyperpiliated and only had a modest ~1 log restoration in NT when compared to the *pilT*^{WA,R35E} *pilU*^{WT} (**Fig. 3b-c**). To more rigorously examine the

stability of these putative intermolecular salt bridges, we performed all-atom molecular dynamics (MD) simulations of the PilT-PilU AF3 model. The resulting 500-ns MD simulations were then analyzed to determine the percent of time that residues remained in close enough proximity to form a salt bridge (<3.5Å), with a higher percentage indicating a more stable interaction. The AF3-MD simulations indicated that PilT^{R35} was not predicted to form a stable interaction with either PilU^{D366} or PilU^{E368} (**Fig. 3d**, **S6**, and **Movie S1**). Thus, while PilT^{R35} is clearly critical for PilT-PilU-dependent retraction, it likely does not form a salt bridge with PilU. Instead, PilT^{R35} may promote PilT-PilU interactions via other intermolecular contacts. Accordingly, the MD simulation suggests that PilT^{R35} interacts with PilU^{I365} and PilU^{M367} (**Fig. S7** and **Movie S2**).

For PilT^{K36}, the AF3-MD simulation predicted a stable salt bridge for PilT^{K36}-PilU^{D366} but not PilT^{K36}-PilU^{E368} (**Fig. 3d**, **S6**, and **Movie S3**). Consistent with this, introducing *pilU^{D366K}* into the *pilT^{K36E}* background restored T4P retraction to parent levels (**Fig. 3b-c**). Furthermore, *pilU^{E368K}* did not restore the T4P retraction deficit of *pilT^{K36E}* (**Fig. 3b-c**), which further highlights the specificity of the PilT^{K36}-PilU^{D366} salt bridge and the residue-level accuracy of the AF3-MD analysis.

For PilT^{D2,E53}, the AF3-MD simulation predicted a stable salt bridge between PilT^{D2,E53}-PilU^{K348}, with all three residues participating in the interaction (**Fig. 3d**, **S6**, and **Movie S4**). Accordingly, *pilT^{WA,D2K,E35R} pilU^{K348D}* largely restored NT and surface piliation when compared to *pilT^{WA,D2K,E35R} pilU^{WT} and pilT^{WA} pilU^{K348D}* (**Fig. 3b-c**).

Together, these results help further validate the AF3 model and demonstrate that PilT-PilU$^{C\text{-term}}$ interactions are critical for PilT-PilU-dependent retraction at the molecular scale.

PilT-PilU$^{C\text{-term}}$ contacts are necessary for NT under physiologically relevant conditions

Thus far, we have used the *pilT^{WA}* background to isolate and study PilT-PilU-dependent retraction, but when PilT ATPase activity is intact, PilU is dispensable for competence T4P retraction. Accordingly, Δ*pilU* can take up soluble transforming DNA (tDNA) from the environment at a similar frequency to the parent (**Fig. 2b** and **4a**). PilU, however, is critical for generating high retraction forces (18, 20). We recently demonstrated that PilU-dependent retraction is necessary for NT when tDNA is adsorbed to a chitin surface (24), a finding that we recapitulate here (**Fig. 4b-c**). Thus, assessing NT of *V. cholerae* in chitin biofilms under flow allows us to study PilT-PilU-dependent retraction in a physiologically relevant setting.

Based on the results described above, we hypothesized that PilT-PilU$^{C\text{-term}}$ contacts would be critical for coordinating the forceful T4P retraction required for NT in chitin flow biofilms when tDNA is adsorbed to chitin. Consistent with this, *pilT^{R35E}*, the single charge-flip mutation that had the strongest impact on PilT-PilU-dependent retraction (**Fig. 2b**), exhibited a loss in NT that was indistinguishable from Δ*pilU* when tDNA was adsorbed to chitin (**Fig. 4b-c**). By contrast, *pilT^{R35E}* did not impact NT when DNA was freely accessible (**Fig. 4a**), suggesting that PilT-PilU$^{C\text{-term}}$ contacts are specifically required for forceful T4P retraction. Together, these results indicate that

PilT-PilU$^{C\text{-}term}$ contacts are critical for these motors to coordinate under physiologically relevant conditions where forceful T4P retraction is necessary for DNA uptake.

PilT-PilU$^{C\text{-}term}$ contacts are important for T4P retraction in Acinetobacter baylyi

PilU is broadly conserved among gammaproteobacteria including, but not limited to, *Acinetobacter baylyi*, *Pseudomonas aeruginosa*, *Legionella pneumophila*, and *Xylella fastidiosa* (**Fig. S4a**). So, we next sought to determine whether PilT-PilU$^{C\text{-}term}$ contacts are a conserved mechanism for PilT-PilU coordination in diverse T4P systems. Sequence alignments highlight that while the majority of PilU$^{C\text{-}term}$ is not conserved, the PilU$_{Vc}^{K348}$ residue that forms a salt bridge with PilT$_{Vc}^{D2,E53}$ is conserved among PilU homologs (**Fig. S4a**). Accordingly, the PilT$_{Vc}^{D2,E53}$-PilU$_{Vc}^{K348}$ salt bridge is conserved in AF3 predictions of PilT-PilU homologs (**Fig. S4b**).

Acinetobacter baylyi competence T4P represent another well-established model system for studying T4P (18, 25, 34-37). For this T4P system, NT is also a simple and sensitive readout (~4-logs of dynamic range) for pilus retraction (**Fig. 5b**). In addition, prior work demonstrates that *pilU$_{Ab}$* is critical for T4P retraction in a *pilT$_{Ab}^{WA}$* background (18), a finding that we recapitulate here (**Fig. 5b**).

The PilT$_{Ab}^{D2,D53}$-PilU$_{Ab}^{K351}$ contact in *A. baylyi* (**Fig. 5a**) is equivalent to the PilT$_{Vc}^{D2,E53}$-PilU$_{Vc}^{K348}$ salt bridge that facilitates PilT-PilU-dependent retraction in *V. cholerae* (**Fig. S4a-b**). To test whether PilT-PilU$^{C\text{-}term}$ contacts are also required for the coordination of these motor ATPases in *A. baylyi*, we targeted the PilT$_{Ab}^{D2,D53}$-PilU$_{Ab}^{K351}$ interface for mutational analysis. Flipping the charge on either side of the interface (*pilT^{WA,D2K,D53R} pilU^{WT}* or *pilT^{WA} pilU^{K351}*) results in an NT deficit that is similar to Δ*pilU* (**Fig. 5b**). And flipping the charge on both sides of the interface (*pilT^{WA,D2K,D53R} pilU^{K351}*) partially (~1.5-log) restores NT (**Fig 5b**), which strongly suggests that these residues form a salt bridge. Together, these results indicate that PilT-PilU$^{C\text{-}term}$ contacts are a conserved mechanism for PilT-PilU coordination in diverse T4P.

DISCUSSION

While prior work established that PilU requires PilT to facilitate retraction (18, 19), a molecular explanation for this interdependence was lacking. Here, we show that PilT is required to "bridge" PilU interactions with the T4P machine *in vivo*. By contrast, PilT could engage T4P machines even in the absence of PilU. PilT homologs contain a highly conserved "AIRNLIRE" motif at the C-terminus (**Fig. S4**) (38). The PilT-PilC AF3 model places the AIRNLIRE motif within the PilT-PilC interface (**Fig. S8**)(39), suggesting that it may be required for PilT-PilC interactions. Interestingly, the AIRNLIRE motif is not conserved among PilU homologs (**Fig. S4**), which may be one reason why PilU does not directly engage the PilC platform. Our results also provide insight into *how* PilT and PilU interact to coordinate retraction. Specifically, we show that interactions between PilT and the PilU$^{C\text{-}term}$, a feature that is unique to PilU homologs (**Fig. S4**), is critical for these proteins to promote T4P retraction. The strong conservation between PilT and PilU indicates that PilU likely arose through duplication of PilT and subsequent evolution of the resulting paralog (12, 40, 41). Thus, it is tempting to speculate that the emergence of PilT-PilU coordination required loss of the "AIRNLIRE" motif and gain of the C-terminal extension in PilU.

While our results show that PilT-PilU$^{C\text{-}term}$ interactions are critical for motor coordination, it is important to acknowledge that this is likely only one of the many molecular interactions required for these motors to coordinate. Prior work demonstrates that T4P motor ATPases likely adopt a C2 symmetry and undergo dynamic conformational changes throughout their catalytic cycle (12, 42). AF3, however, only models PilT and PilU with C6 symmetry, highlighting that these models cannot provide insight into the molecular interactions required for motor coordination throughout the PilT-PilU catalytic cycle. Future work will focus on integrating the catalytic dynamics of these motor proteins with the PilT-PilU$^{C\text{-}term}$ interactions identified in our study.

Motor ATPase coordination is a prevalent feature among diverse T4P systems. Several gammaproteobacteria encode PilT and PilU homologs (**Fig S4**), and we demonstrate that PilT-PilU$^{C\text{-}term}$ contacts are a conserved mechanism for PilT-PilU coordination in *A. baylyi*. Outside of the gammaproteobacteria, some species encode multiple PilT paralogs (*e.g.*, *Neisseria spp.* and *Myxococcus spp.*), suggesting that motor ATPase coordination may also be conserved in more distantly related T4P systems. Additionally, some T4P rely on multiple motor ATPases for pilus extension (34, 43), suggesting that motor coordination may be a critical feature of both T4P extension and retraction.

While our results provide insight into the molecular coordination between PilT-PilU, it remains unclear why this coordination is necessary. PilU is required to generate high retraction forces (18, 20), which are required for some T4P activities (20, 24). Here, we show that PilT-PilU likely form stacked hexamers that are arranged head-to-tail. Also, we show that the PilU$^{C\text{-}term}$ binds to the sides of the PilT hexamer in a manner that could allow PilU to "pull" on PilT during its catalytic cycle. It is tempting to speculate that this arrangement allows these motors to intimately coordinate their catalytic cycles to combine their efforts and generate forces that could not be achieved by either motor alone. To explore this idea, we sought to estimate the maximum force that a single T4P retraction ATPase can generate (see **Methods** for details). This estimate is derived from four main assumptions: 1) that the free energy of ATP hydrolysis under physiological conditions is -47 kJ/mol (44), 2) that two molecules of ATP are hydrolyzed per catalytic cycle (12, 42), 3) that each catalytic cycle removes one pilin subunit from the pilus filament resulting in a step size of 1 nm (13, 45), and 4) that AAA+ motor ATPases like PilT/PilU operate at an efficiency of ~32.5% (46, 47). Based on this, we estimate that a single T4P retraction motor can generate ~50 pN of force. T4P, however, have empirically been shown to retract at force that exceeds 100 pN (48-50). Thus, the molecular coordination between PilT-PilU we show here may, in fact, be necessary to achieve the high T4P retraction forces observed in nature.

METHODS

Bacterial strains and culture conditions

Vibrio cholerae and *Acinetobacter baylyi* strains were routinely grown in LB broth and on LB agar plates. Medium was supplemented with kanamycin (50 µg/mL), spectinomycin (200µg/mL), sulfamethoxazole (100µg/mL), trimethoprim (10µg/mL), carbenicillin (100µg/mL),

and chloramphenicol (1µg/mL) when appropriate. A comprehensive list of strains used in this study can be found in **Table S1**.

Natural Transformation (NT) assays

Chitin-independent NT assays of *V. cholerae* were conducted using strains where 1) TfoX, the master competence regulator, was placed under an IPTG-inducible promoter (P_{tac}-*tfoX*), and 2) *luxO* was deleted to genetically lock cells in a high-density state. To induce natural competence, strains were grown to late-log by rolling at 30 °C in LB supplemented with 20 mM $MgCl_2$, 10 mM $CaCl_2$, and 100 µM IPTG. Then, 7 µL of this culture was diluted into 350 µL of Instant Ocean medium (IO; 7 g/L Aquarium Systems) for each transformation reaction. Two reactions were setup for each strain: one where 100 ng of tDNA (a ΔVC1807::Kan^R PCR product) was added and a negative control where no DNA was added. After 3 min of tDNA incubation, 6 units of DNase I (NEB) was added to stop DNA uptake, and reactions were incubated overnight at 30 °C to allow for tDNA integration. The next day, 0.5 mL LB was added, and reactions were outgrown at 37 °C shaking for 3 hrs. Reactions were then dribble plated for quantitative culture on LB plates with kanamycin (to quantify transformant CFUs) and on plain LB agar plates (to quantify total CFUs). The transformation frequency was determined by dividing the CFUs of transformants by the total CFUs. For reactions with no transformants, the limit of detection was calculated and plotted.

Chitin-dependent NT assays of *V. cholerae* in the presence of soluble DNA or chitin adsorbed DNA were conducted exactly as previously described (24). Briefly, strains contained two fluorescent reporters: a disrupted GFP construct (ΔVC1807::Cm^R-*lacI*-P_{tac}-*gfp::parST1*) and a constitutively expressed mKate2 construct (Δ*lacZ*::$Spec^R$-*lacI*-P_{tac}-*mKate2*).

For assays where free DNA was supplied, strains were grown rolling at 30 °C in LB to mid-log. Cells were then washed and adjusted to an OD_{600} = 1.0 in IO. Next, chitin-dependent transformation reactions were setup by mixing the following in a 2mL eppi: 100 µL of cells, 150 µL chitin slurry (8 g / 150 mL IO; Alfa Aesar), and 750 µL IO. Two reactions were prepped for each strain. Reactions were incubated static overnight at 30 °C to induce natural competence. The next day, 1000 ng of tDNA (a ΔVC1807::Cm^R-*lacI*-P_{tac}-*gfp* PCR product) was added to one reaction, while no DNA was added to the other reaction, which served as a negative control. All reactions were incubated overnight at 30 °C with shaking to ensure the tDNA remained in solution. The next day, cells were harvested from the chitin, placed under a 0.4% IO gelzan pad and imaged via epifluorescence microscopy with FITC and mCherry filter cubes. Images were analyzed using MicrobeJ to determine the number of mKate (total) and GFP (transformant) fluorescent cells. Transformation frequency was calculated by dividing the GFP (transformant) cell counts by the mKate (total) cell counts (at least 500 cells analyzed in each sample).

For assays where tDNA was chitin adsorbed, flow cells (24) containing chitin flakes were first washed with 0.13 ng/µL of tDNA (a ΔVC1807::Cm^R-*lacI*-P_{tac}-*gfp* PCR product) at a volumetric flow rate of 0.1 µL/min for 24 h. Following this tDNA adsorption step, the flow cell inlet tubing was swapped to blank defined artificial seawater (DASW; consists of 234 mM NaCl, 27.5 mM MgSO4, 1.5 mM NaHCO3, 4.95 mM CaCl2, 5.15 mM KCl, 0.07 mM Na2B4O7, 0.05 mM SrCl, 0.015 mM NaBr, 0.001 mM NaI, 0.013 mM LiCl, 0.187 mM K2HPO4, and pH 7.1

triethanolamine) and flow was maintained at 0.1 µL/min for an additional 24 h to remove any unbound tDNA. After this wash step, 100 µL of reporter cells were resuspended in DASW to an OD_{600} of 5.0 and inoculated into the chambers via syringe, after which flow with blank DASW was resumed. The reporter strain was then incubated at room temperature (~22°C) for 48 h before imaging. Flow cells were imaged using a Zeiss 880 line-scanning confocal microscope and a 40x/1.2 N.A. water objective. A 488 nm laser line was used to excite the GFP protein expressed after transformation events and a 594 nm laser line was used to excite the mKate2 protein carried by the reporter strain. BiofilmQ was used to threshold images and quantify the reporter (mKate2 labeled) and transformant (GFP labeled) biovolumes (51). The transformation frequency was calculated as GFP biovolume divided by mKate2 biovolume. For samples where no transformants were observed, the approximate biovolume of a single cell was used to calculate the limit of detection and plotted.

For NT assays of *A. baylyi*, overnight cultures were washed and adjusted to an OD_{600} = 2.0 in fresh LB. Then, 50 µL of this culture was added to 450 µL LB supplemented with 20mM $MgCl_2$ and 10mM $CaCl_2$ in a 2 mL eppi. Two transformation reactions were setup for each strain: one where 50 ng of tDNA (a ΔACIAD1551::Kan^R PCR product) was added and a negative control where no tDNA was added. Transformations were incubated with end-over-end rotation at 30 °C for 45 mins. After 45 min of tDNA incubation, 6 units of DNase I (NEB) was added to stop DNA uptake, and reactions were incubated with end-over-end rotation at 30 °C for an additional 5 hrs to allow for tDNA integration and outgrowth. Reactions were then dribble plated for quantitative culture on LB plates with kanamycin (to quantify transformant CFUs) and on plain LB agar plates (to quantify total CFUs). The transformation frequency was determined by dividing the CFUs of transformants by the total CFUs. For reactions with no transformants, the limit of detection was calculated and plotted.

Construction of mutant strains

All *V. cholerae* strains used in this study were derivatives of the El Tor isolate E7946 (52). All *A. baylyi* strains were derivatives of strain ADP1 (53). All mutant strains were generated by NT (as described above). Mutant constructs were generated by splicing-by-overlap-extension (SOE) exactly as previously described (54-56). A list of all primers used to generate mutant constructs can be found in **Table S2**.

Microscopy

Unless otherwise indicated, phase and epifluorescence (FITC, YFP, mCherry channels) images were collected on an inverted Nikon Ti-2 microscope with a Plan Apo ×60 objective fitted with a Hamamatsu ORCAFlash 4.0 camera using Nikon NIS Elements imaging software.

Motor localization assay

For these assays, all *V. cholerae* strains contained the P_{tac}-*tfoX* and Δ*luxO* mutations required for chitin-independent induction of competence as describe above for NT assays. Cells were grown overnight in LB supplemented with 20 mM $MgCl_2$, 10 mM $CaCl_2$, and 100 µM IPTG rolling at 30 °C. The next day, 500 µL of overnight culture was subcultured into 3 mL of LB supplemented with 20 mM $MgCl_2$, 10 mM $CaCl_2$, and 100 µM IPTG and grown for 1 hr rolling at 30 °C. Then,

100 µL of this culture was spun down and washed in IO. Cells were then placed under a 0.4% IO gelzan pad and imaged via timelapse microscopy (2 sec intervals for 10 sec duration) with the phase contrast and mCherry channels. Quantification of fluorescent foci was performed using MicrobeJ features detection. Foci were only counted if they were stable (moved less than 0.3 µm throughout the duration of the timelapse) and were present in all frames of the timelapse.

For quantification of co-localizing foci, cells were imaged via timelapse microscopy (2 sec intervals for 10 sec duration) with the phase contrast, YFP, and mCherry channels. MicrobeJ features detection was used to identify cells with stable GFP-PilU foci. Then, the presence of a co-localizing PilT-mCherry focus was determined manually. Results are presented as the percentage of the population that had co-localizing foci.

Pilus labeling and imaging

V. cholerae strains were grown exactly as described above for chitin-independent NT assays. Then, 100 µL of late-log cells were pelleted at 8000 x g for 1 min and washed in IO. Cells were then labeled with 25 µg/mL AF488-mal for 15 mins static at room temperature. Cells were then washed three times in IO, ensuring to spin at 8000 x g for 1 min to prevent shearing of surface pili. Cells were then placed under a 0.4% IO gelzan pad and imaged with the phase and FITC channels. Representative images of the piliation phenotype for each strain were selected from the raw microscopy images.

T4P-dependent aggregation assay

V. cholerae strains were grown exactly as described above for chitin-independent NT assays. Subcultures were allowed to sit static at room temperature on the benchtop for 15 mins to let cellular aggregates settle out of solution. Representative images were taken of each strain without disturbing settled cells.

AF3-MD analysis

The initial structure of the PilT-PilU complex was generated using AlphaFold 3 (28). Propka3 was used to assign the charges of the ionizable residues and the protonation state of histidine residues (57). $PilU^{D253}$ and $PilU^{E280}$ were protonated. Based on their local electrostatic environment, $PilT^{H151}$, $PilT^{H166}$, $PilT^{H183}$, $PilT^{H229}$, $PilT^{H280}$, $PilU^{H164}$, $PilU^{H240}$, and $PilU^{H276}$ were set to histidine-epsilon (HSE). All other histidine residues were set to histidine-delta (HSD).

The PilT-PilU structure was subsequently solvated, using CHARMM-GUI, v3.7 generating a 162$Å^3$ water box (58, 59). Potassium (K^+) and chloride (Cl^-) ions were added in order to neutralize the system as well as produce an ionic strength of 150 mM Simulations were conducted with NAMD3 (60) using the CHARMM36m protein force field (61), and TIP3P water model (62). The initial structure was minimized for 10,000 steps, followed by a two-stage equilibration: first, 1ns of MD was run while restraining the protein heavy atoms, and second, 4ns of MD was run while restraining only the protein backbones, thereby equilibrating the box dimensions. Production runs were performed using hydrogen mass repartitioning (HMR), allowing for a uniform 4 fs time step (63, 64).

The simulations were run at a constant temperature (310 K) and constant isotropic pressure (1 atm), maintained by a Langevin thermostat and piston, respectively (65). Long-range electrostatics were calculated at every time step using the particle-mesh Ewald method (66). We set a short-range cutoff for Lennard-Jones interactions at 12 Å with a switching function starting at 10 Å. Two independent replicas were performed for 500 ns.

Animations were rendered with VMD v1.9.4a51 (67), and the distance calculations were performed with MDAnalysis (68, 69), where the minimum distance between two residue side chains was taken as the closest pair of heavy atoms. In the case where multiple interactions are considered (e.g. $PilT^{R35}$-$PilU^{D366,E368}$), the minimum distance was taken for either residue in the target pair. Salt bridges and contacts were defined when this distance was less than a cutoff of 3.5 Å or 4.5 Å, respectively.

Estimating T4P force generation

The following equation was used to calculate the maximal force (F_{max}) generated by a T4P motor ATPase:

$$F_{max} = \frac{Energy\ consumed\ (J)}{Step\ size\ (m)}$$

The energy consumed was determined based on two assumptions: 1) the free energy of ATP hydrolysis in physiological conditions is -47 kJ/mol (44) and 2) that two molecules of ATP are hydrolyzed per ATPase cycle (12, 42). Based on this, the free energy released upon hydrolysis of two ATP molecules was determined to be 1.56×10^{-19} J. To estimate the step size, we assumed that one pilin is removed from the pilus filament in each ATPase cycle resulting in a step size of 1 nm (or 1×10^{-9} m) (13, 45). These values were then plugged into the equation above to calculate the F_{max} generated by T4P motors at 100% efficiency:

$$F_{max} = \frac{1.56 \text{ x } 10^{-19} \text{ J}}{1 \text{ x } 10^{-9}\ m} = 1.56 \text{ x } 10^{-10}\ N = 156 \text{ pN}$$

It is unlikely that these motor proteins operate at 100% efficiency. Prior work has defined the efficiencies of two other members of the AAA+ family of motor ATPases: the phi29 packing motor = 30% (46) and ClpX = 35% (47). We averaged these values (32.5%) to generate an estimate for the efficiency of this family of motor ATPases. Accounting for average efficiency, we estimated that a single T4P motor can maximally generate ~50.7 pN of force.

Generating multiple sequence alignments

Multiple sequence alignments (MSA) were generated by first gathering the PilT and PilU protein sequences from each organism from GenBank. Sequences were then aligned using T-Coffee (70), and the alignments were reformatted for the final figure using the Sequence Manipulation Suite: Color Align Conservation tool (71).

Summary Statistics

See **Dataset S1** for summary statistics for all quantitative data in this manuscript.

ACKNOLWEDGEMENTS

We would like to thank Marc Morais and Jennifer Chlebek for helpful discussions. This work was supported by the National Institutes of Health (NIH) through grants R35GM128674 to ABD, R01GM148586 to JCG, and R35GM151158 to CDN.

REFERENCES

1. P. Seitz, M. Blokesch, DNA-uptake machinery of naturally competent Vibrio cholerae. *Proc Natl Acad Sci U S A* **110**, 17987-17992 (2013).
2. C. Pujol, E. Eugene, M. Marceau, X. Nassif, The meningococcal PilT protein is required for induction of intimate attachment to epithelial cells following pilus-mediated adhesion. *Proc Natl Acad Sci U S A* **96**, 4017-4022 (1999).
3. C. K. Ellison *et al.*, Obstruction of pilus retraction stimulates bacterial surface sensing. *Science* **358**, 535-538 (2017).
4. A. J. Merz, M. So, M. P. Sheetz, Pilus retraction powers bacterial twitching motility. *Nature* **407**, 98-102 (2000).
5. J. M. Skerker, H. C. Berg, Direct observation of extension and retraction of type IV pili. *Proc Natl Acad Sci U S A* **98**, 6901-6904 (2001).
6. I. Guilvout *et al.*, Membrane platform protein PulF of the Klebsiella type II secretion system forms a trimeric ion channel essential for endopilus assembly and protein secretion. *mBio* **15**, e0142323 (2024).
7. M. McCallum, S. Tammam, J. L. Rubinstein, L. L. Burrows, P. L. Howell, CryoEM map of Pseudomonas aeruginosa PilQ enables structural characterization of TsaP. *Structure* **29**, 457-466 e454 (2021).
8. Y. W. Chang *et al.*, Architecture of the type IVa pilus machine. *Science* **351**, aad2001 (2016).
9. S. J. Weaver *et al.*, CryoEM structure of the type IVa pilus secretin required for natural competence in Vibrio cholerae. *Nat Commun* **11**, 5080 (2020).
10. M. Wolfgang, J. P. van Putten, S. F. Hayes, D. Dorward, M. Koomey, Components and dynamics of fiber formation define a ubiquitous biogenesis pathway for bacterial pili. *EMBO J* **19**, 6408-6418 (2000).
11. C. K. Ellison *et al.*, Retraction of DNA-bound type IV competence pili initiates DNA uptake during natural transformation in Vibrio cholerae. *Nat Microbiol* **3**, 773-780 (2018).
12. M. McCallum, S. Tammam, A. Khan, L. L. Burrows, P. L. Howell, The molecular mechanism of the type IVa pilus motors. *Nat Commun* **8**, 15091 (2017).
13. L. Craig *et al.*, Type IV pilus structure by cryo-electron microscopy and crystallography: implications for pilus assembly and functions. *Mol Cell* **23**, 651-662 (2006).
14. C. B. Whitchurch, M. Hobbs, S. P. Livingston, V. Krishnapillai, J. S. Mattick, Characterisation of a Pseudomonas aeruginosa twitching motility gene and evidence for a specialised protein export system widespread in eubacteria. *Gene* **101**, 33-44 (1991).
15. M. Wolfgang, H. S. Park, S. F. Hayes, J. P. van Putten, M. Koomey, Suppression of an absolute defect in type IV pilus biogenesis by loss-of-function mutations in pilT, a

twitching motility gene in Neisseria gonorrhoeae. *Proc Natl Acad Sci U S A* **95**, 14973-14978 (1998).
16. H. S. Park, M. Wolfgang, M. Koomey, Modification of type IV pilus-associated epithelial cell adherence and multicellular behavior by the PilU protein of Neisseria gonorrhoeae. *Infect Immun* **70**, 3891-3903 (2002).
17. C. B. Whitchurch, J. S. Mattick, Characterization of a gene, pilU, required for twitching motility but not phage sensitivity in Pseudomonas aeruginosa. *Mol Microbiol* **13**, 1079-1091 (1994).
18. J. L. Chlebek *et al.*, PilT and PilU are homohexameric ATPases that coordinate to retract type IVa pili. *PLoS Genet* **15**, e1008448 (2019).
19. D. W. Adams, J. M. Pereira, C. Stoudmann, S. Stutzmann, M. Blokesch, The type IV pilus protein PilU functions as a PilT-dependent retraction ATPase. *PLoS Genet* **15**, e1008393 (2019).
20. J. Thongchol *et al.*, Removal of Pseudomonas type IV pili by a small RNA virus. *Science* **384**, eadl0635 (2024).
21. P. Seitz *et al.*, ComEA is essential for the transfer of external DNA into the periplasm in naturally transformable Vibrio cholerae cells. *PLoS Genet* **10**, e1004066 (2014).
22. A. B. Dalia, T. N. Dalia, Spatiotemporal Analysis of DNA Integration during Natural Transformation Reveals a Mode of Nongenetic Inheritance in Bacteria. *Cell* **179**, 1499-1511 e1410 (2019).
23. K. L. Meibom, M. Blokesch, N. A. Dolganov, C. Y. Wu, G. K. Schoolnik, Chitin induces natural competence in Vibrio cholerae. *Science* **310**, 1824-1827 (2005).
24. J. D. Holt, Y. Peng, T. N. Dalia, A. B. Dalia, C. D. Nadell, Environmental DNA adsorption to chitin can promote horizontal gene transfer by natural transformation. *Proc Natl Acad Sci U S A* **122**, e2420708122 (2025).
25. J. L. Chlebek, R. Denise, L. Craig, A. B. Dalia, Motor-independent retraction of type IV pili is governed by an inherent property of the pilus filament. *Proc Natl Acad Sci U S A* **118** (2021).
26. E. Couser, J. L. Chlebek, A. B. Dalia, Retraction ATPase Motors from Three Orthologous Type IVa Pilus Systems Support Promiscuous Retraction of the Vibrio cholerae Competence Pilus. *J Bacteriol* **204**, e0012622 (2022).
27. D. W. Adams, S. Stutzmann, C. Stoudmann, M. Blokesch, DNA-uptake pili of Vibrio cholerae are required for chitin colonization and capable of kin recognition via sequence-specific self-interaction. *Nat Microbiol* 10.1038/s41564-019-0479-5 (2019).
28. J. Abramson *et al.*, Accurate structure prediction of biomolecular interactions with AlphaFold 3. *Nature* **630**, 493-500 (2024).
29. P. Chiang *et al.*, Functional role of conserved residues in the characteristic secretion NTPase motifs of the Pseudomonas aeruginosa type IV pilus motor proteins PilB, PilT and PilU. *Microbiology (Reading)* **154**, 114-126 (2008).
30. K. A. Floyd *et al.*, c-di-GMP modulates type IV MSHA pilus retraction and surface attachment in Vibrio cholerae. *Nat Commun* **11**, 1549 (2020).
31. H. Q. Hughes *et al.*, Nitric oxide stimulates type IV MSHA pilus retraction in Vibrio cholerae via activation of the phosphodiesterase CdpA. *Proc Natl Acad Sci U S A* **119** (2022).

32. S. Maggi *et al.*, Integrative Structure and Function of the Vibrio cholerae Competence Pilus Machine. *bioRxiv* 10.1101/2025.10.14.680967 (2025).
33. C. K. Ellison, T. N. Dalia, A. B. Dalia, Y. V. Brun, Real-time microscopy and physical perturbation of bacterial pili using maleimide-conjugated molecules. *Nat Protoc* **14**, 1803-1819 (2019).
34. C. K. Ellison *et al.*, Acinetobacter baylyi regulates type IV pilus synthesis by employing two extension motors and a motor protein inhibitor. *Nat Commun* **12**, 3744 (2021).
35. C. K. Ellison *et al.*, Subcellular localization of type IV pili regulates bacterial multicellular development. *Nat Commun* **13**, 6334 (2022).
36. T. J. Ellison, C. K. Ellison, Improved DNA binding to a type IV minor pilin increases natural transformation. *Nucleic Acids Res* **53** (2025).
37. T. J. Ellison, I. Y. Yen, P. L. Howell, C. K. Ellison, FimX regulates type IV pilus localization via the Pil-Chp chemosensory system in Acinetobacter baylyi. *bioRxiv* 10.1101/2025.05.21.655318 (2025).
38. K. G. Aukema, E. M. Kron, T. J. Herdendorf, K. T. Forest, Functional dissection of a conserved motif within the pilus retraction protein PilT. *J Bacteriol* **187**, 611-618 (2005).
39. C. J. Geiger, G. C. L. Wong, G. A. O'Toole, A bacterial sense of touch: T4P retraction motor as a means of surface sensing by Pseudomonas aeruginosa PA14. *J Bacteriol* **206**, e0044223 (2024).
40. R. Denise, S. S. Abby, E. P. C. Rocha, Diversification of the type IV filament superfamily into machines for adhesion, protein secretion, DNA uptake, and motility. *PLoS Biol* **17**, e3000390 (2019).
41. R. Barnshaw *et al.*, Separation of Pseudomonas aeruginosa type IV pilus-dependent twitching motility and surface-sensing responses. *mBio* 10.1128/mbio.02521-25, e0252125 (2025).
42. M. McCallum *et al.*, Multiple conformations facilitate PilT function in the type IV pilus. *Nat Commun* **10**, 5198 (2019).
43. H. Q. Hughes, N. D. Christman, T. N. Dalia, C. K. Ellison, A. B. Dalia, The PilT retraction ATPase promotes both extension and retraction of the MSHA type IVa pilus in Vibrio cholerae. *PLoS Genet* **18**, e1010561 (2022).
44. Q. H. Tran, G. Unden, Changes in the proton potential and the cellular energetics of Escherichia coli during growth by aerobic and anaerobic respiration or by fermentation. *Eur J Biochem* **251**, 538-543 (1998).
45. H. Ochner *et al.*, Structure of the Pseudomonas aeruginosa PAO1 Type IV pilus. *PLoS Pathog* **20**, e1012773 (2024).
46. D. E. Smith *et al.*, The bacteriophage straight phi29 portal motor can package DNA against a large internal force. *Nature* **413**, 748-752 (2001).
47. R. A. Maillard *et al.*, ClpX(P) generates mechanical force to unfold and translocate its protein substrates. *Cell* **145**, 459-469 (2011).
48. B. Maier *et al.*, Single pilus motor forces exceed 100 pN. *Proc Natl Acad Sci U S A* **99**, 16012-16017 (2002).
49. M. Clausen, V. Jakovljevic, L. Sogaard-Andersen, B. Maier, High-force generation is a conserved property of type IV pilus systems. *J Bacteriol* **191**, 4633-4638 (2009).

50. M. D. Koch, M. E. Black, E. Han, J. W. Shaevitz, Z. Gitai, Pseudomonas aeruginosa distinguishes surfaces by stiffness using retraction of type IV pili. *Proc Natl Acad Sci U S A* **119**, e2119434119 (2022).
51. R. Hartmann *et al.*, Quantitative image analysis of microbial communities with BiofilmQ. *Nat Microbiol* **6**, 151-156 (2021).
52. V. L. Miller, V. J. DiRita, J. J. Mekalanos, Identification of toxS, a regulatory gene whose product enhances toxR-mediated activation of the cholera toxin promoter. *J Bacteriol* **171**, 1288-1293 (1989).
53. E. Juni, A. Janik, Transformation of Acinetobacter calco-aceticus (Bacterium anitratum). *J Bacteriol* **98**, 281-288 (1969).
54. A. B. Dalia, Natural Cotransformation and Multiplex Genome Editing by Natural Transformation (MuGENT) of Vibrio cholerae. *Methods Mol Biol* **1839**, 53-64 (2018).
55. A. B. Dalia, E. McDonough, A. Camilli, Multiplex genome editing by natural transformation. *Proc Natl Acad Sci U S A* **111**, 8937-8942 (2014).
56. A. B. Dalia, D. W. Lazinski, A. Camilli, Characterization of undermethylated sites in Vibrio cholerae. *J Bacteriol* **195**, 2389-2399 (2013).
57. M. H. Olsson, C. R. Sondergaard, M. Rostkowski, J. H. Jensen, PROPKA3: Consistent Treatment of Internal and Surface Residues in Empirical pKa Predictions. *J Chem Theory Comput* **7**, 525-537 (2011).
58. S. Jo, T. Kim, V. G. Iyer, W. Im, CHARMM-GUI: a web-based graphical user interface for CHARMM. *J Comput Chem* **29**, 1859-1865 (2008).
59. J. Lee *et al.*, CHARMM-GUI Input Generator for NAMD, GROMACS, AMBER, OpenMM, and CHARMM/OpenMM Simulations Using the CHARMM36 Additive Force Field. *J Chem Theory Comput* **12**, 405-413 (2016).
60. J. C. Phillips *et al.*, Scalable molecular dynamics on CPU and GPU architectures with NAMD. *J Chem Phys* **153**, 044130 (2020).
61. J. Huang *et al.*, CHARMM36m: an improved force field for folded and intrinsically disordered proteins. *Nat Methods* **14**, 71-73 (2017).
62. W. L. Jorgensen, J. Chandrasekhar, J. D. Madura, R. W. Impey, M. L. Klein, Comparison of Simple Potential Functions for Simulating Liquid Water. *Journal of Chemical Physics* **79**, 926-935 (1983).
63. C. W. Hopkins, S. Le Grand, R. C. Walker, A. E. Roitberg, Long-Time-Step Molecular Dynamics through Hydrogen Mass Repartitioning. *J Chem Theory Comput* **11**, 1864-1874 (2015).
64. C. Balusek *et al.*, Accelerating Membrane Simulations with Hydrogen Mass Repartitioning. *J Chem Theory Comput* **15**, 4673-4686 (2019).
65. S. E. Feller, Y. H. Zhang, R. W. Pastor, B. R. Brooks, Constant-Pressure Molecular-Dynamics Simulation - the Langevin Piston Method. *Journal of Chemical Physics* **103**, 4613-4621 (1995).
66. T. Darden, D. York, L. Pedersen, Particle Mesh Ewald - an N.Log(N) Method for Ewald Sums in Large Systems. *Journal of Chemical Physics* **98**, 10089-10092 (1993).
67. W. Humphrey, A. Dalke, K. Schulten, VMD: visual molecular dynamics. *J Mol Graph* **14**, 33-38, 27-38 (1996).

68. N. Michaud-Agrawal, E. J. Denning, T. B. Woolf, O. Beckstein, MDAnalysis: a toolkit for the analysis of molecular dynamics simulations. *J Comput Chem* **32**, 2319-2327 (2011).
69. M. L. R. J. Gowers, J. Barnoud, T. J. E. Reddy, M. N. Melo, S. L. Seyler, D. L. Dotson, J. Domanski, S. Buchoux, I. M. Kenney, and O. Beckstein, MDAnalysis: A Python package for the rapid analysis of molecular dynamics simulations. *Proceedings of the 15th Python in Science Conference* 10.25080/Majora-629e541a-00e, 98-105 (2016).
70. C. Notredame, D. G. Higgins, J. Heringa, T-Coffee: A novel method for fast and accurate multiple sequence alignment. *J Mol Biol* **302**, 205-217 (2000).
71. P. Stothard, The sequence manipulation suite: JavaScript programs for analyzing and formatting protein and DNA sequences. *Biotechniques* **28**, 1102, 1104 (2000).

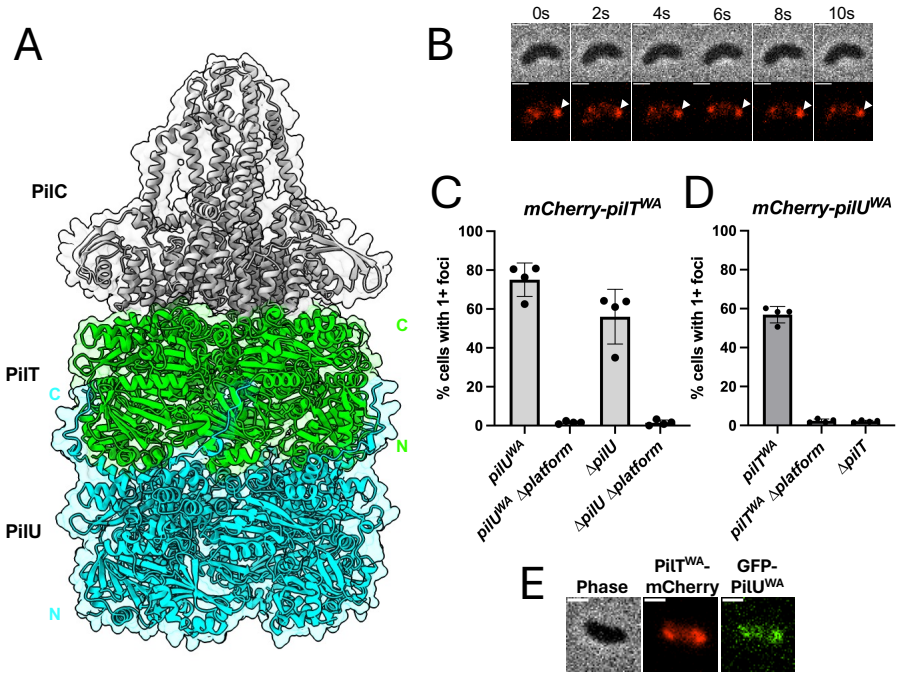

Fig. 1. **PilT bridges PilU to the T4P machine.** (**A**) A hybrid AlphaFold 3 model highlights the putative interactions between PilC (grey), PilT (green), and PilU (cyan). The N-terminal and C-terminal faces of PilT and PilU are labeled with green and cyan letters, respectively. Motor localization assays were performed to assess the localization of PilT and PilU *in vivo* by epifluorescence time lapse microscopy in **B**-**D**. (**B**) A representative montage of timelapse imaging for a *V. cholerae* cell expressing mCherry-PilT^{WA} that displayed a stable ATPase focus (white carat). Scale bar, 1µm. For quantification in these assays, a fluorescent focus was only counted if it was maintained throughout the duration of the 10-s timelapse. (**C**) Motor localization assay of cells expressing *mCherry-pilT^{WA}* (WA = the *pilT^{K136A}* Walker A mutation that ablates ATPase activity) and the indicated mutations. The Δ*platform* mutation denotes a mutant lacking both the competence T4P platform *pilC* and the MSHA T4P platform *mshG*. For each strain, the percentage of cells (*n* = 120 cells analyzed) with one or more fluorescent mCherry-PilT^{WA} foci is reported. (**D**) Motor localization assay of cells expressing *mCherry-pilU^{WA}* (WA = the *pilU^{K134A}* Walker A mutation that ablates ATPase activity) and the indicated mutations. For each strain, the percentage of cells (*n* = 120 cells analyzed) with one or more fluorescent mCherry-PilU^{WA} foci is reported. (**E**) Motor localization assay of cells expressing *pilT^{WA}-mCherry gfp-pilU^{WA}*. The representative image shows PilT^{WA}-mCherry and GFP-PilU^{WA} co-localization (GFP-PilU^{WA} foci co-localize with PilT^{WA}-mCherry foci at a frequency of 96% ± 2%). Data in **C**-**E** are from 4 independent biological replicates and shown as the mean ± SD.

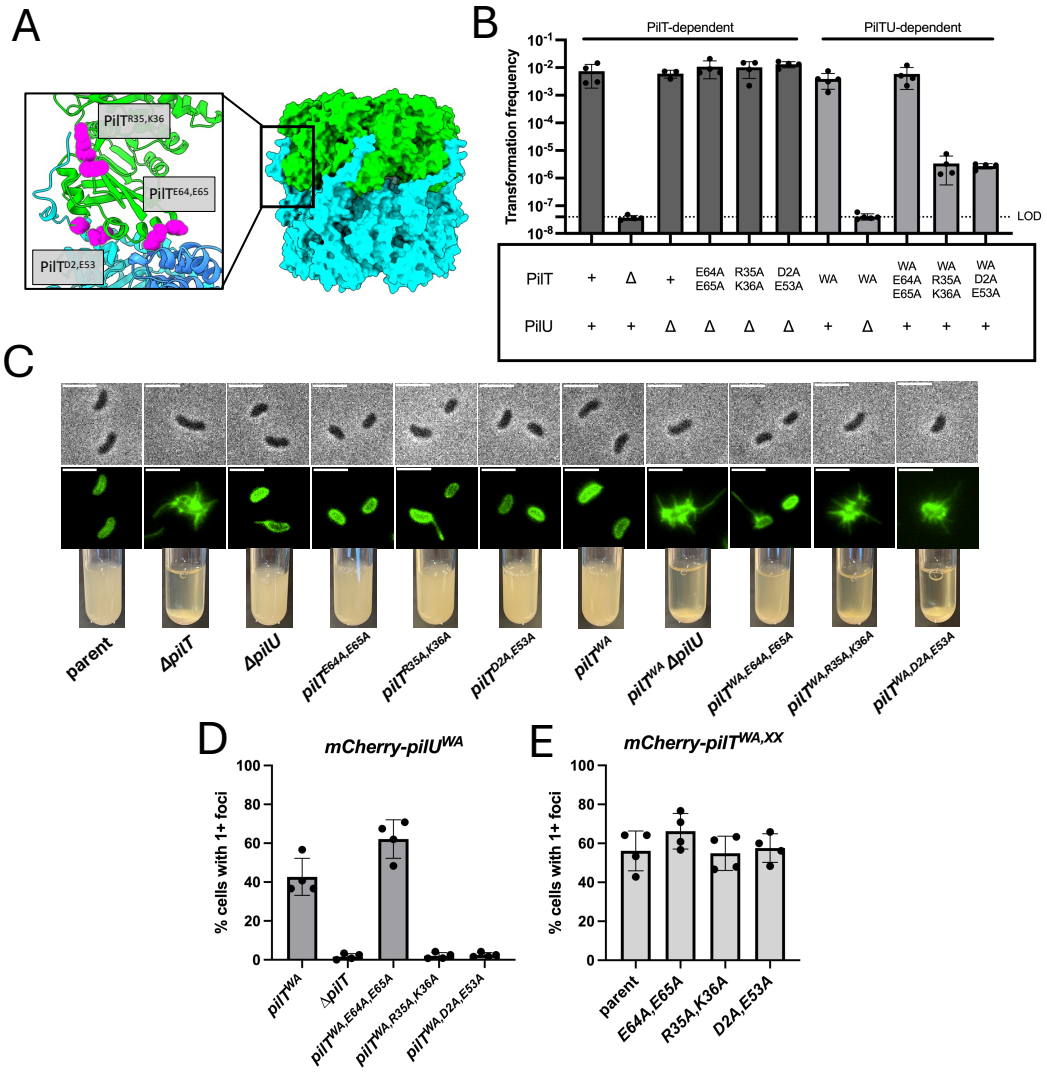

Fig. 2. **Contacts between PilT and the PilU$^{C\text{-term}}$ are critical for PilT-PilU interactions and T4P retraction.** (**A**) AF3 model of PilT (green)-PilU (cyan) interactions. Inset highlights the interaction interfaces targeted for mutagenesis. The PilT residues that putatively participate in intermolecular salt bridges are shown in magenta. (**B**) NT assays of the indicated *V. cholerae* strains. Dark gray bars denote strains that report on PilT-dependent retraction (*i.e.*, in a *pilT*$^{+}$ background where PilT ATPase activity is intact), while light grey bars denote strains that report on PilT-PilU-dependent retraction (*i.e.*, in a *pilT*^{WA} background where retraction is dependent on PilU). (**C**) Representative images of surface piliation (top panel) and cellular aggregation (bottom panel) for the indicated strains. Scale bars on micrographs, 3μm. Data are representative of two independent experiments. (**D**) Motor localization assay of cells expressing *mCherry-pilU*^{WA} and the indicated *pilT* alleles. For each strain, the percentage of cells (n = 120 cells analyzed) with one or more fluorescent mCherry-PilU^{WA} foci is reported. (**E**) Motor localization assay of Δ*pilU* cells expressing an *mCherry-pilT*^{WA} construct with the additional mutations indicated. For each strain, the percentage of cells (n = 120 cells analyzed) with one or more fluorescent mCherry-PilT^{WA} foci is reported. Data in **B**, **D**, and **E** are from 4 independent biological replicates and shown as the mean ± SD.

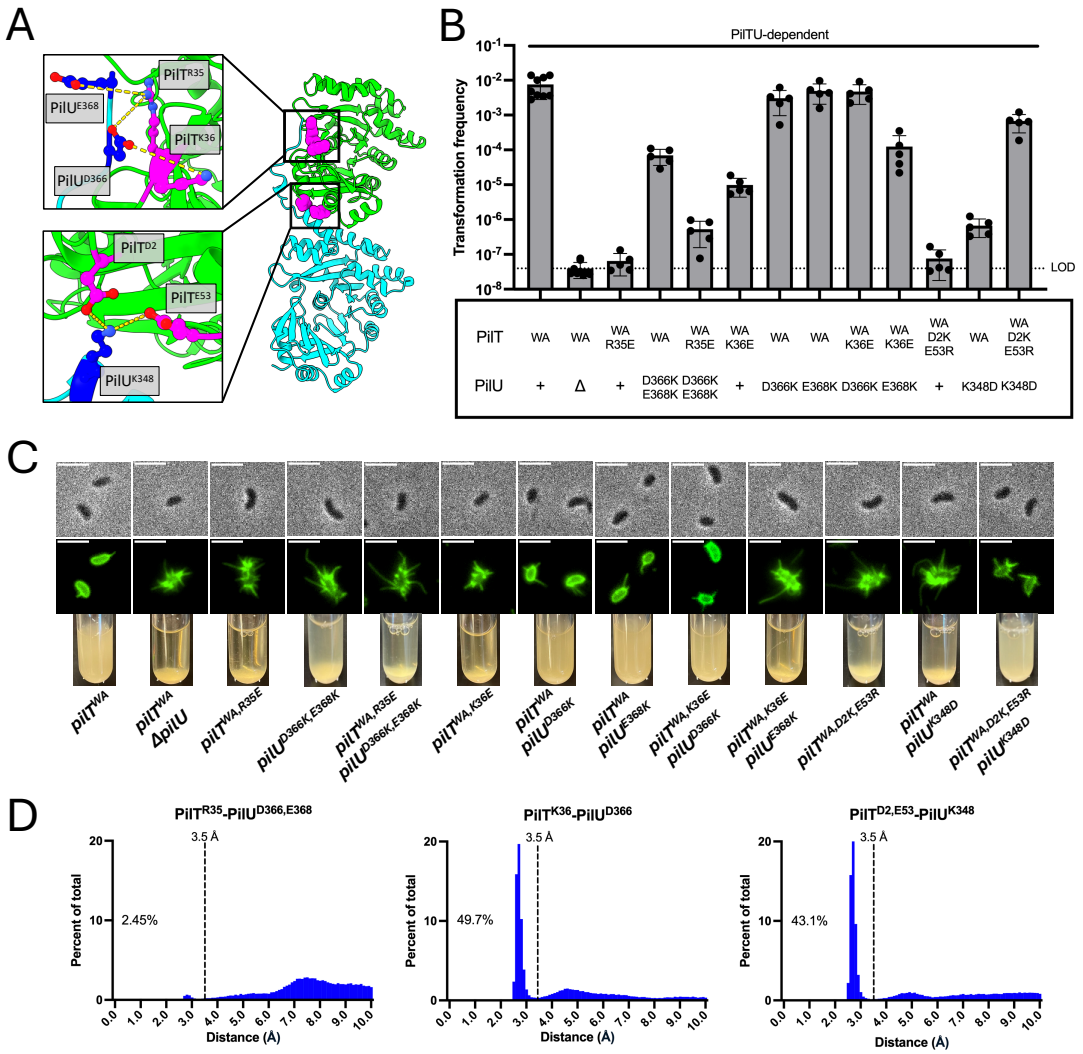

Fig. 3. **AF3-MD simulations and high-resolution genetic analysis reveal PilT-PilU$^{C\text{-term}}$ salt bridges required for motor coordination.** (**A**) AF3 model of PilT (green)-PilU (cyan) interactions. The inset highlights the residues that participate in the three putative salt bridges targeted for mutagenesis. PilT residues are shown in magenta with nitrogen atoms colored blue, and PilU residues are shown in dark blue with oxygen atoms colored red. (**B**) NT assay of the indicated *V. cholerae* strains. Data are from five independent biological replicates and shown as the mean ± SD. (**C**) Representative images of surface piliation (top panel) and cellular aggregation (bottom panel) for the indicated strains. Scale bar for micrographs, 3μm. Data are representative of two independent experiments. (**D**) Distance frequency histogram for the indicated residue pairs during the MD simulation of the AF3 PilT-PilU model. Distances between the side chains of the indicated residues were measured at 0.1-ns intervals over the 500-ns simulation. Percentage on graph denotes the amount of time that the indicated side chains are <3.5Å (dotted line). Data are compiled from two independent MD simulations.

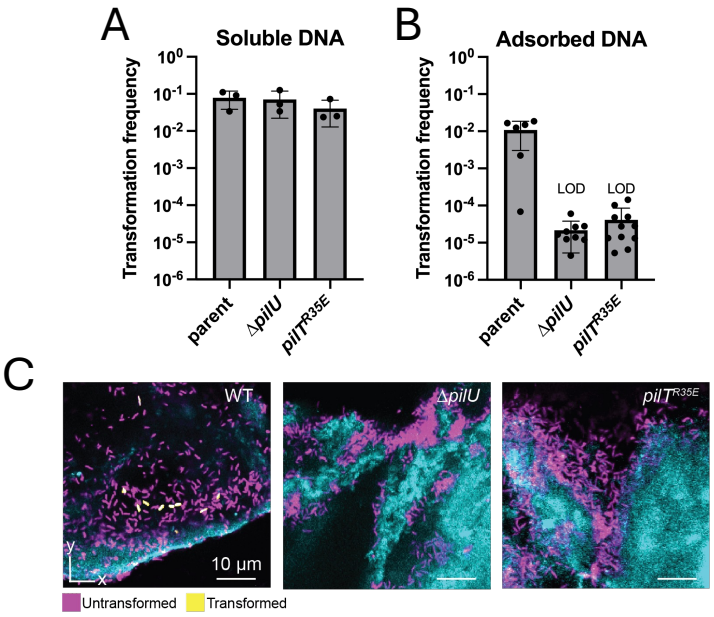

Fig. 4. **PilT-PilU$^{C\text{-}term}$ interactions are critical for motor coordination under physiologically relevant conditions.** (**A**) Chitin-dependent NT assays of the indicated *V. cholerae* strains with soluble tDNA. (**B**) Flow biofilm NT assays where tDNA was adsorbed to the chitin surface. (**C**) Representative images of assays described in **B** highlighting transformed (yellow) and untransformed (magenta) cells within the chitin-bound biofilm. The chitin surface is shown in cyan and appears irregular in shape due to optical sectioning through the 3-dimensional shrimp shell particles used for these experiments. All data are from at least 3 independent biological replicates and shown as the mean ± SD.

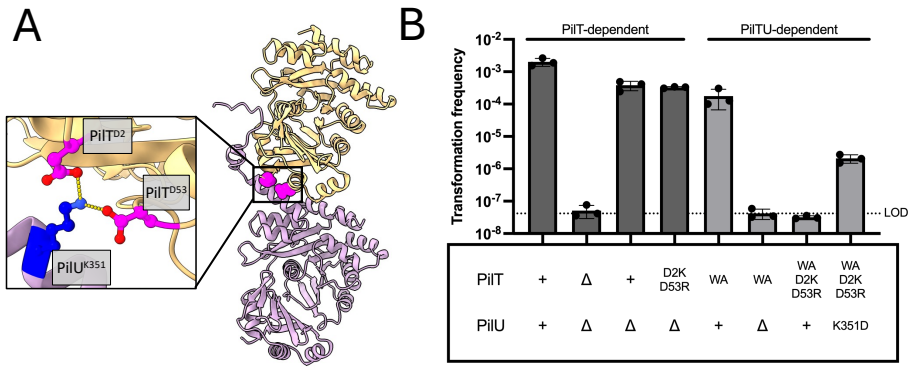

Fig. 5. **PilT-PilU$^{C\text{-}term}$ contacts are important for T4P retraction in *A. baylyi*.** (**A**) AF3 model of PilT$_{Ab}$ (orange)-PilU$_{Ab}$ (pink) interactions. Inset shows the conserved PilT$_{Ab}^{D2,D53}$-PilU$_{Ab}^{K351}$ salt bridge. (**B**) NT assays of the indicated *A. baylyi* strains. Dark gray bars denote strains that report on PilT-dependent retraction (*i.e.*, in a *pilT*$^{+}$ background where PilT ATPase activity is intact), while light grey bars denote strains that report on PilT-PilU-dependent retraction (*i.e.*, in a *pilT*^{WA} background where retraction is dependent on PilU). Data are from three independent biological replicates and shown as the mean ± SD.

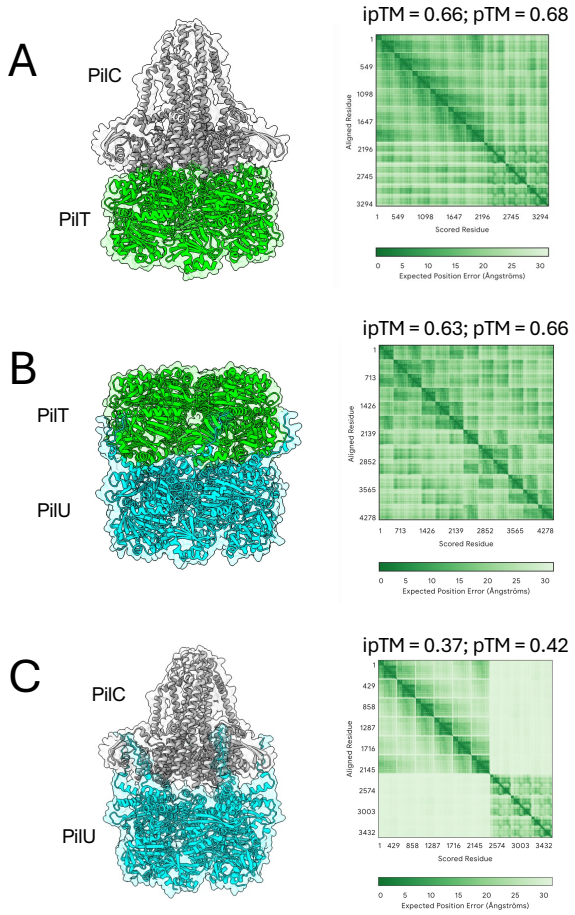

Fig. S1. **AF3 models of PilT-PilC, PilT-PilU, and PilU-PilC interactions.** AF3 models (left) of the indicated *V. cholerae* proteins with their respective PAE maps and confidence scores (right). (**A**) PilT(x6)-PilC(x3) and (**B**) PilT(x6)-PilU(x6) were used to generate the PilC-PilT-PilU hybrid complex shown in **Fig. 1A.** (**C**) The PilU(x6)-PilC(x3) AF3 model had very low confidence metrics, suggesting that these proteins may not directly interact.

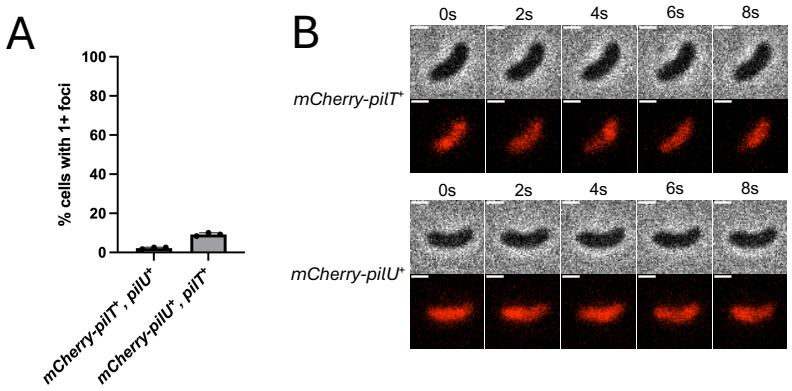

Fig. S2. **PilT and PilU fusions do not form stable fluorescent foci when their ATPase activity is intact.** (**A**) Motor localization assays were performed on the indicated *V. cholerae* strains. "+" denotes that the indicated motor protein has its ATPase activity intact. For each strain, the percentage of cells (n = 120 cells analyzed) with one or more fluorescent mCherry foci is reported. Data are from three independent biological replicates and are shown as the mean ± SD. (**B**) Representative montage of timelapse imaging for the indicated strains highlights the lack of stable fluorescent foci in these backgrounds. Scale bars, 1μM.

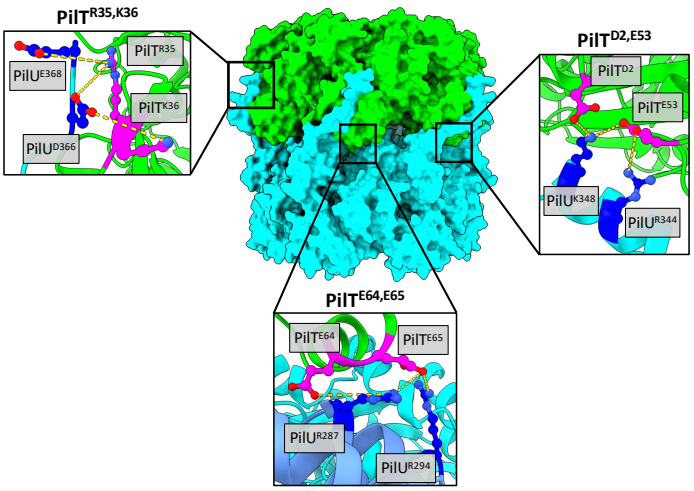

Fig. S3. Contact analysis of the AF3 PilT-PilU model reveals three putative intermolecular salt bridges. AF3 model of the PilT (green)-PilU (cyan) complex. Insets show the residues involved in the three putative intermolecular salt bridges with PilT residues colored in magenta and PilU residues colored in blue.

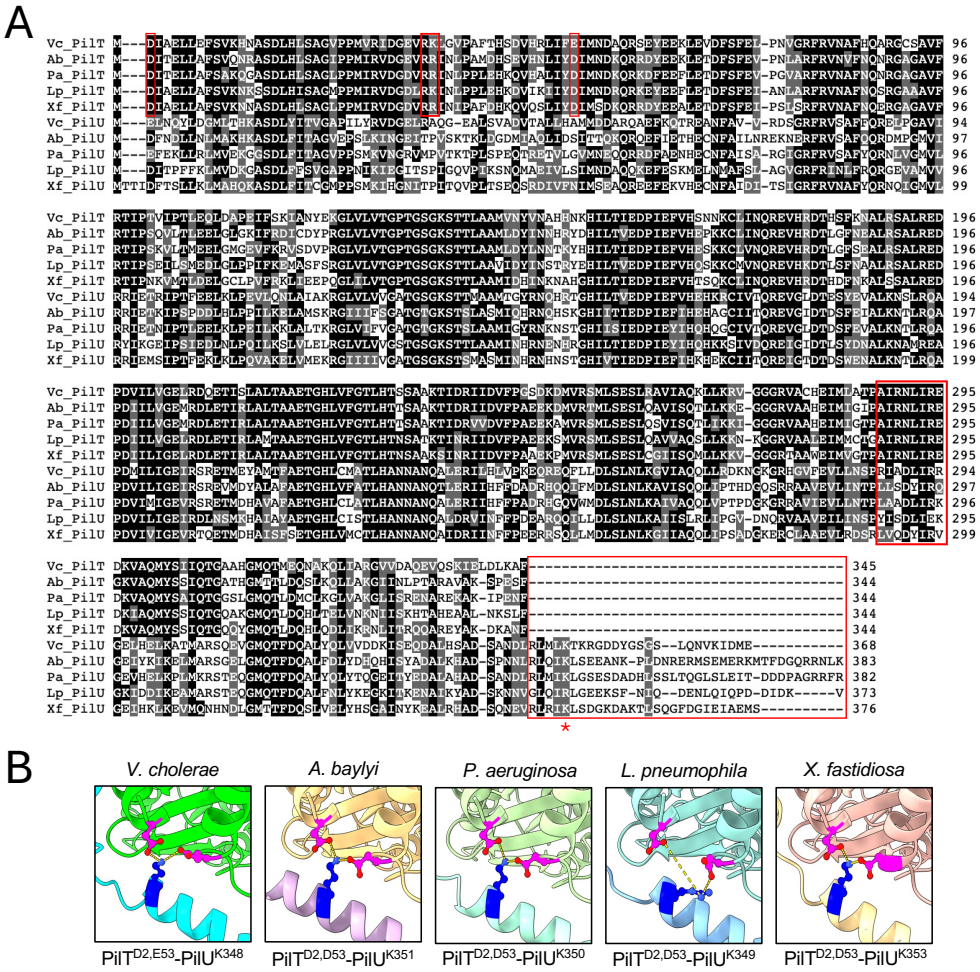

Fig. S4. Sequence and structural alignments uncover conserved elements in PilT and PilU homologs. (**A**) Multiple sequence alignment of PilT and PilU homologs from the following bacterial species: Vc = *Vibrio cholerae*, Ab = *Acinetobacter baylyli*, Pa = *Pseudomonas aeruginosa*, Lp = *Legionella pneumophila*, and Xf = *Xylella fastidiosa*. Red boxes denote conservation of the $PilT_{Vc}$ residues studied (D2, R35, K36, and E53), the PilT AIRNLIRE motif, and the extended C-terminus that is unique to PilU homologs. The red asterisk highlights conservation of the $PilU_{Vc}^{K348}$ residue among PilU homologs. (**B**) AF3 models of PilT-PilU complexes from the indicated species highlights the predicted conservation of the experimentally validated $PilT_{Vc}^{D2,E53}$-$PilU_{Vc}^{K348}$ interfacial salt bridge.

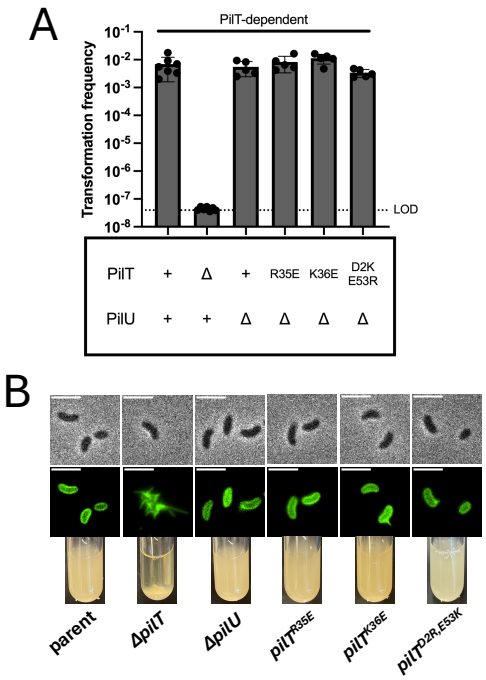

Fig. S5. Mutating the PilT residues in the putative interfacial salt bridges does not impact PilT-dependent retraction. (**A**) NT assays of the indicated *V. cholerae* strains demonstrates that mutating the residues involved in putative PilT-PilU interfacial salt bridges does not impact PilT-dependent retraction (*i.e.*, in a background where PilT ATPase activity is intact). Data are from five independent biological replicates and shown as the mean ± SD. (**B**) Representative images of surface piliation (top panel) and cellular aggregation (bottom panel) for the indicated strains. Scale bar for micrographs, 3μm. Data are representative of two independent experiments.

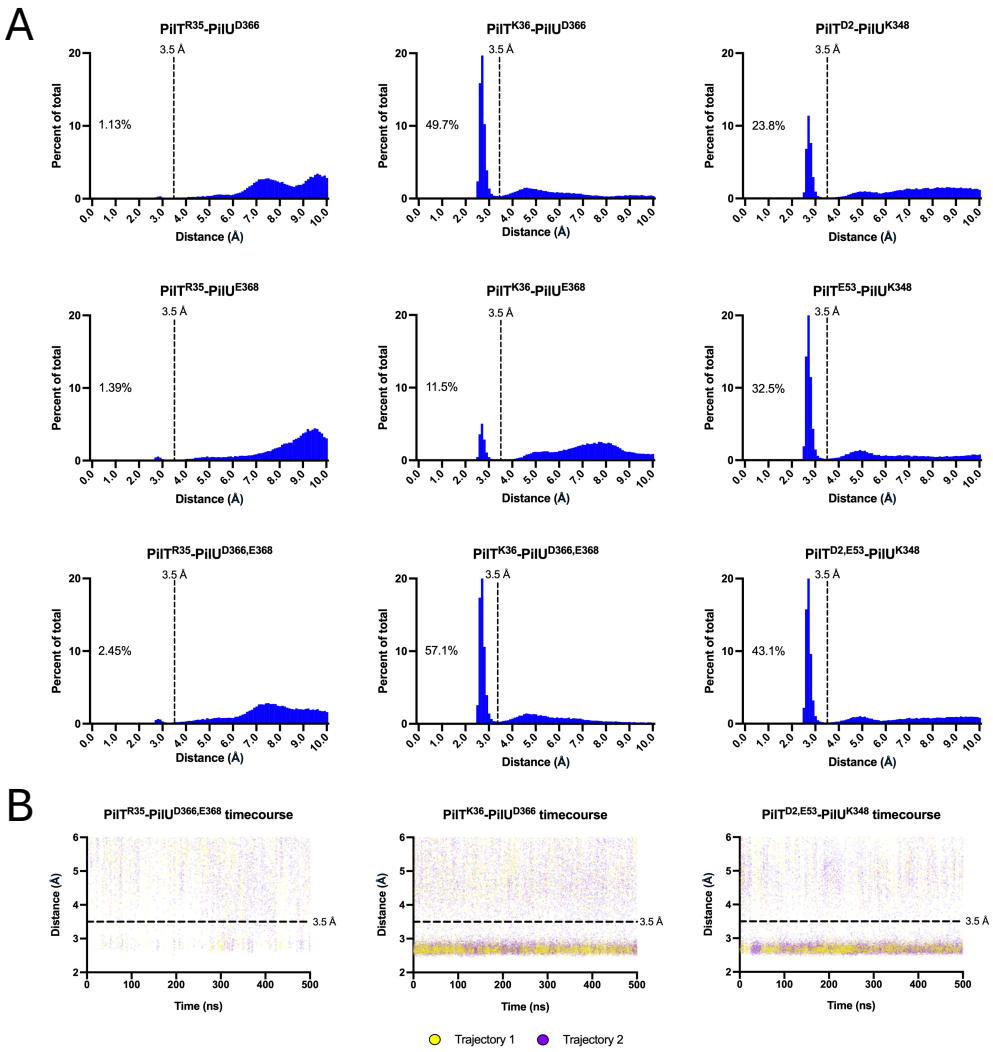

Fig. S6. MD simulations of the AF3 PilT-PilU complex predict stable salt bridges between PilT^{K36}-PilU^{D366} and PilT^{D2,E53}-PilU^{K348}. (**A**) Distance frequency histogram for the indicated residue pairs during the MD simulation of the AF3 PilT-PilU model. Distances between the side chains of the indicated residues were measured at 0.1-ns intervals over the 500 ns simulation. Percentage on graph denotes the amount of time that the indicated side chains are <3.5Å (dotted line). Data are compiled from two independent MD simulations. (**B**) Time-course scatter plots of distance measurements for the indicated residue pairs. Trajectories 1 and 2 represent two independent replicates of the MD simulations.

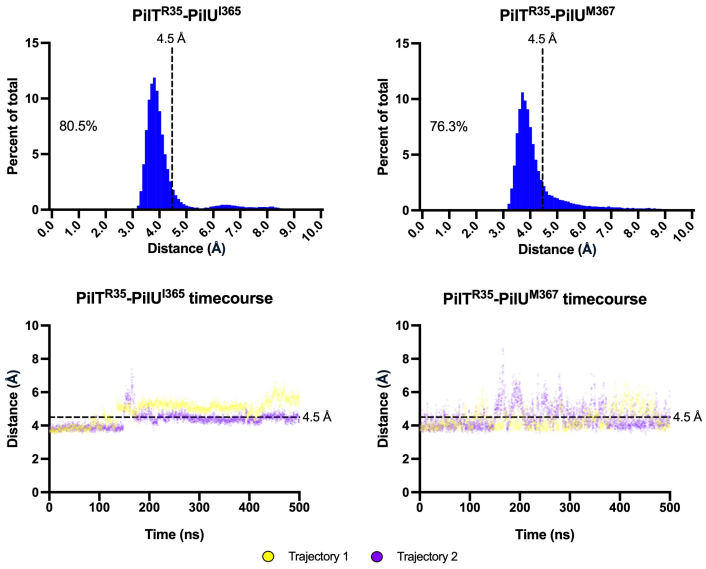

Fig. S7. AF3-MD simulations support PilT^{R35}-PilU^{I365,M367} interactions. (**A**) Distance histograms of the indicated residues. Distances between the side chains of the indicated residues were recorded at 0.1-ns intervals over the 500-ns MD simulation. Percentages denote the amount of time that the residues were within 4.5Å (dotted line). Data are compiled from two independent MD simulations. (**B**) Time-course scatter plots of the distance measurements for the indicated interactions. Trajectories 1 and 2 represent two independent replicates of the MD simulation.

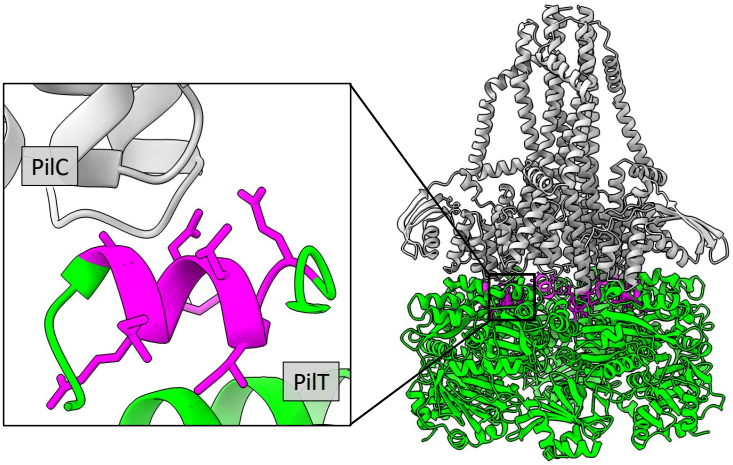

Fig. S8. AF3 predicts that the AIRNLIRE motif is at the PilC-PilT interface. AF3 model of the PilC(3x)-PilT(6x) complex. Residues of the AIRNLIRE motif (PilT$^{A288-E295}$) are colored in magenta. The inset shows a slice of the PilT-PilC model for a better view of the AIRNLIRE motif at the PilC-PilT interface.

Table S1. Strains used in this study

Strain #	Genotype	Figure	Use in manuscript	Name in manuscript
AET249 / SAD4023	E7946 Sm^R, P_{tac}-*tfoX*, Δ*luxO*, *pilA*^{S67C}, Δ*pilT*::Smx^R *pilU*^{K134A}, Δ*lacZ*::$Spec^R$-P_{pilT}-*mCherry*-L5-*pilT*^{K136A}	Fig 1c	Fluorescence microscopy foci quantification	*mCherry-pilT*^{WA}, *pilU*^{WA}
AET396 / SAD4024	E7946 Sm^R, P_{tac}-*tfoX*, Δ*luxO*, *pilA*^{S67C}, Δ*pilT*::SmxR *pilU*^{K134A}, Δ*lacZ*::$Spec^R$-P_{pilT}-*mCherry*-L5-*pilT*^{K136A}, Δ*MSHA*::$Carb^R$, Δ*pilC*::Cm^R	Fig 1c	Fluorescence microscopy foci quantification	*mCherry-pilT*^{WA}, *pilU*^{WA}, Δ*platform*
AET146 / SAD4025	E7946 Sm^R, P_{tac}-*tfoX*, Δ*luxO*, *pilA*^{S67C}, Δ*lacZ*::$Spec^R$-P_{pilT}-*mCherry*-L5-*pilT*^{K136A}, Δ*pilTU*::Tm^R	Fig 1c; Fig 2e	Fluorescence microscopy foci quantification	*mCherry-pilT*^{WA}, Δ*pilU*
AET222 / SAD4026	E7946 *Sm*^{R}, P_{tac}-*tfoX*, Δ*luxO*, *pilA*^{S67C}, Δ*lacZ*::$Spec^R$-P_{pilT}-*mCherry*-L5-*pilT*^{K136A}, Δ*pilTU*::Tm^R, Δ*MSHA*::$Carb^R$, Δ*pilC*::Cm^R	Fig 1c	Fluorescence microscopy foci quantification	*mCherry-pilT*^{WA}, Δ*pilU,* Δ*platform*
AET159 / SAD4027	E7946 Sm^R, P_{tac}-*tfoX*, Δ*luxO*, *pilA*^{S67C}, Δ*pilT*::Smx^R *mCherry*-L5-*pilU*^{K134A}, Δ*lacZ*::$Spec^R$-P_{pilT}-*pilT*^{K136A}	Fig 1d; Fig 2d	Fluorescence microscopy foci quantification	*mCherry-pilU*^{WA}, *pilT*^{WA}
AET205 / SAD4028	E7946 Sm^R, P_{tac}-*tfoX*, Δ*luxO*, *pilA*^{S67C}, Δ*pilT*::Smx^R *mCherry*-L5-*pilU*^{K134A}, Δ*lacZ*::$Spec^R$-P_{pilT}-*pilT*^{K136A}, Δ*MSHA*::$Carb^R$, Δ*pilC*::Cm^R	Fig 1d	Fluorescence microscopy foci quantification	*mCherry-pilU*^{WA}, *pilT*^{WA}, Δ*platform*
AET153 / SAD4029	E7946 Sm^R, P_{tac}-*tfoX*, Δ*luxO*, *pilA*^{S67C}, Δ*pilT*::Smx^R *mCherry*-L5-*pilU*^{K134A}	Fig 1d; Fig 2d	Fluorescence microscopy foci quantification	*mCherry-pilU*^{WA}, Δ*pilT*
AET155 / SAD4030	E7946 Sm^R, P_{tac}-*tfoX*, Δ*luxO*, *pilA*^{S67C}, Δ*pilT*::Smx^R *gfp*-L5-*pilU*^{K134A}, Δ*lacZ*::$Spec^R$-P_{pilT}-*pilT*^{K136A}-L5-*mCherry*	Fig 1e	Fluorescence co-localization	*pilT*^{WA}*-mCherry, gfp-pilU*^{WA}
TND0905 / SAD2468 / (18, 26)	E7946 Sm^R, P_{tac}-*tfoX*, Δ*luxO*, *pilA*^{S67C}	Fig 2b-c; Fig S5a-b	Transformation, pilus labeling, and cellular aggregation assays	Parent
AET111 / SAD4031	E7946 Sm^R, P_{tac}-*tfoX*, Δ*luxO*, *pilA*^{S67C}, Δ*pilT*::Smx^R	Fig 2b-c; Fig S5a-b	Transformation, pilus labeling, and cellular aggregation assays	Δ*pilT*
TND1515 / SAD4032	E7946 Sm^R, P_{tac}-*tfoX*, Δ*luxO*, *pilA*^{S67C}, Δ*pilU*::Tm^R	Fig 2b-c; Fig S5a-b	Transformation, pilus labeling, and cellular aggregation assays	Δ*pilU*

TND4516 / SAD4033	E7946 Sm^R, P_{tac}-*tfoX*, Δ*luxO*, *pilA*^{S67C}, Δ*pilT*::Smx^R, Δ*lacZ*::$Spec^R$-PpilT-*pilT*^{K136A}	Fig 2b-c; Fig 3b-c	Transformation, pilus labeling, and cellular aggregation assays	*pilT*^{WA}
TND4360 / SAD4034	E7946 Sm^R, P_{tac}-*tfoX*, Δ*luxO*, *pilA*^{S67C}, Δ*pilTU*::Tm^R, Δ*lacZ*::$Spec^R$-P_{pilT}-*pilT*^{K136A}	Fig 2b-c; Fig 3b-c	Transformation, pilus labeling, and cellular aggregation assays	*pilT*^{WA}, Δ*pilU*
TND4361 / SAD4035	E7946 Sm^R, P_{tac}-*tfoX*, Δ*luxO*, *pilA*^{S67C}, Δ*pilTU*::Tm^R, Δ*lacZ*::$Spec^R$-P_{pilT}-*pilT*^{E64A,E65A}	Fig 2b-c	Transformation, pilus labeling, and cellular aggregation assays	*pilT*^{E64A,E65A}
TND4362 / SAD4036	E7946 Sm^R, P_{tac}-*tfoX*, Δ*luxO*, *pilA*^{S67C}, Δ*pilTU*::Tm^R, Δ*lacZ*::$Spec^R$-P_{pilT}-*pilT*^{R35A,K36A}	Fig 2b-c	Transformation, pilus labeling, and cellular aggregation assays	*pilT*^{R35A,K36A}
AET265 / SAD4037	E7946 Sm^R, P_{tac}-*tfoX*, Δ*luxO*, *pilA*^{S67C}, Δ*pilTU*::Tm^R, Δ*lacZ*::$Spec^R$-P_{pilT}-*pilT*^{D2A,E53A}	Fig 2b-c	Transformation, pilus labeling, and cellular aggregation assays	*pilT*^{D2A,E53A}
AET112 / SAD4038	E7946 Sm^R, P_{tac}-*tfoX*, Δ*luxO*, *pilA*^{S67C}, Δ*pilT*::Smx^R, Δ*lacZ*::$Spec^R$-P_{pilT}-*pilT*^{E64A,E65A,K136A}	Fig 2b-c	Transformation, pilus labeling, and cellular aggregation assays	*pilT*^{WA,E64A,E65A}
AET113 / SAD4039	E7946 Sm^R, P_{tac}-*tfoX*, Δ*luxO*, *pilA*^{S67C}, Δ*pilT*::Smx^R, Δ*lacZ*::$Spec^R$-P_{pilT}-*pilT*^{R35A,K36A,K136A}	Fig 2b-c	Transformation, pilus labeling, and cellular aggregation assays	*pilT*^{WA,R35A,K36A}
AET275 / SAD4040	E7946 Sm^R, P_{tac}-*tfoX*, Δ*luxO*, *pilA*^{S67C}, Δ*pilT*::Smx^R, Δ*lacZ*::$Spec^R$-P_{pilT}-*pilT*^{D2A,E53A,K136A}	Fig 2b-c	Transformation, pilus labeling, and cellular aggregation assays	*pilT*^{WA,D2A,E53A}
AET262 / SAD4041	E7946 Sm^R, P_{tac}-*tfoX*, Δ*luxO*, *pilA*^{S67C}, Δ*pilT*::Smx^R *mCherry*-L5-*pilU*^{K134A}, Δ*lacZ*::$Spec^R$-P_{pilT}-*pilT*^{E64A,E65A,K136A}	Fig 2d	Fluorescence microscopy foci quantification	*mCherry-pilU*^{WA}, *pilT*^{WA,E64A,E65A}
AET263 / SAD4042	E7946 Sm^R, P_{tac}-*tfoX*, Δ*luxO*, *pilA*^{S67C}, Δ*pilT*::Smx^R *mCherry*-L5-*pilU*^{K134A}, Δ*lacZ*::$Spec^R$-P_{pilT}-*pilT*^{R35A,K36A,K136A}	Fig 2d	Fluorescence microscopy foci quantification	*mCherry-pilU*^{WA}, *pilT*^{WA,R35A,K36A}
AET277 / SAD4043	E7946 Sm^R, P_{tac}-*tfoX*, Δ*luxO*, *pilA*^{S67C}, Δ*pilT*::Smx^R *mCherry*-L5-*pilU*^{K134A}, Δ*lacZ*::$Spec^R$-P_{pilT}-*pilT*^{D2A,E53A,K136A}	Fig 2d	Fluorescence microscopy foci quantification	*mCherry-pilU*^{WA}, *pilT*^{WA,D2A,E53A}
AET271 / SAD4044	E7946 Sm^R, P_{tac}-*tfoX*, Δ*luxO*, *pilA*^{S67C}, Δ*pilTU*::Tm^R, Δ*lacZ*::$Spec^R$-P_{pilT}-*mCherry*-L5-*pilT*^{E64A,E65A,K136A}	Fig 2e	Fluorescence microscopy foci quantification	*mCherry-pilT*$^{WA,E64A\ E65A}$

AET270 / SAD4045	E7946 Sm^R, P_{tac}-*tfoX*, Δ*luxO*, *pilA*^{S67C}, Δ*pilTU*::Tm^R, Δ*lacZ*::$Spec^R$-P_{pilT}-*mCherry*-L5-*pilT*^{R35A,K36A,K136A}	Fig 2e	Fluorescence microscopy foci quantification	*mCherry-pilT*$^{WA,R35A\ K36A}$
AET278 / SAD4046	E7946 Sm^R, P_{tac}-*tfoX*, Δ*luxO*, *pilA*^{S67C}, Δ*pilTU*::Tm^R, Δ*lacZ*::$Spec^R$-P_{pilT}-*mCherry*-L5-*pilT*^{D2A,E53A,K136A}	Fig 2e	Fluorescence microscopy foci quantification	*mCherry-pilT*^{WA,D2A,E53A}
AET189 / SAD4047	E7946 Sm^R, P_{tac}-*tfoX*, Δ*luxO*, *pilA*^{S67C}, Δ*pilT*::Smx^R, Δ*lacZ*::$Spec^R$-P_{pilT}-*pilT*^{R35E,K136A}	Fig 3b-c	Transformation, pilus labeling, and cellular aggregation assays	*pilT*^{WA,R35E}
TND4578 / SAD4048	E7946 Sm^R, P_{tac}-*tfoX*, Δ*luxO*, *pilA*^{S67C}, Δ*pilT*::Smx^R *pilU*^{D366K,E368K}, Δ*lacZ*::$Spec^R$-P_{pilT}-*pilT*^{K136A}	Fig 3b-c	Transformation, pilus labeling, and cellular aggregation assays	*pilT*^{WA}, *pilU*^{D366K,E368K}
AET391 / SAD4049	E7946 Sm^R, P_{tac}-*tfoX*, Δ*luxO*, *pilA*^{S67C}, Δ*pilT*::Smx^R *pilU*^{D366K,E368K}, Δ*lacZ*::$Spec^R$-P_{pilT}-*pilT*^{R35E,K136A}	Fig 3b-c	Transformation, pilus labeling, and cellular aggregation assays	*pilT*^{WA,R35E}, *pilU*^{D366K,E368K}
AET190 / SAD4050	E7946 Sm^R, P_{tac}-*tfoX*, Δ*luxO*, *pilA*^{S67C}, Δ*pilT*::Smx^R, Δ*lacZ*::$Spec^R$-P_{pilT}-*pilT*^{K36E,K136A}	Fig 3b-c	Transformation, pilus labeling, and cellular aggregation assays	*pilT*^{WA,K36E}
AET200 / SAD4051	E7946 Sm^R, P_{tac}-*tfoX*, Δ*luxO*, *pilA*^{S67C}, Δ*pilT*::Smx^R *pilU*^{D366K}, Δ*lacZ*::$Spec^R$-P_{pilT}-*pilT*^{K136A}	Fig 3b-c	Transformation, pilus labeling, and cellular aggregation assays	*pilT*^{WA}, *pilU*^{D366K}
AET201 / SAD4052	E7946 Sm^R, P_{tac}-*tfoX*, Δ*luxO*, *pilA*^{S67C}, Δ*pilT*::Smx^R *pilU*^{E368K}, Δ*lacZ*::$Spec^R$-P_{pilT}-*pilT*^{K136A}	Fig 3b-c	Transformation, pilus labeling, and cellular aggregation assays	*pilT*^{WA}, *pilU*^{E368K}
AET198 / SAD4053	E7946 Sm^R, P_{tac}-*tfoX*, Δ*luxO*, *pilA*^{S67C}, Δ*pilT*::Smx^R *pilU*^{D366K}, Δ*lacZ*::$Spec^R$-P_{pilT}-*pilT*^{K36E,K136A}	Fig 3b-c	Transformation, pilus labeling, and cellular aggregation assays	*pilT*^{WA,K36E}, *pilU*^{D366K}
AET199 / SAD4054	E7946 Sm^R, P_{tac}-*tfoX*, Δ*luxO*, *pilA*^{S67C}, Δ*pilT*::Smx^R *pilU*^{E368K}, Δ*lacZ*::$Spec^R$-P_{pilT}-*pilT*^{K36E,K136A}	Fig 3b-c	Transformation, pilus labeling, and cellular aggregation assays	*pilT*^{WA,K36E}, *pilU*^{E368K}
AET345 / SAD4055	E7946 Sm^R, P_{tac}-*tfoX*, Δ*luxO*, *pilA*^{S67C}, Δ*pilT*::Smx^R, Δ*lacZ*::$Spec^R$-P_{pilT}-*pilT*^{D2K,E53R,K136A}	Fig 3b-c	Transformation, pilus labeling, and cellular aggregation assays	*pilT*^{WA,D2K,E53R}
AET337 / SAD4056	E7946 Sm^R, P_{tac}-*tfoX*, Δ*luxO*, *pilA*^{S67C}, Δ*pilT*::Smx^R *pilU*^{K348D}, Δ*lacZ*::$Spec^R$-P_{pilT}-*pilT*^{K136A}	Fig 3b-c	Transformation, pilus labeling, and cellular aggregation assays	*pilT*^{WA}, *pilU*^{K348D}

AET358 / SAD4057	E7946 Sm^R, P_{tac}-*tfoX*, Δ*luxO*, *pilA*^{S67C}, Δ*pilT*::Smx^R *pilU*^{K348D}, Δ*lacZ*::$Spec^R$-P_{pilT}-*pilT*^{D2K,E53R,K136A}	Fig 3b-c	Transformation, pilus labeling, and cellular aggregation assays	*pilT*^{WA,D2K,E53R}, *pilU*^{K348D}
TND3433 / SAD4058 / (24)	Δ*VC1807*::Cm^R-P_{tac}-*gfp*::*parST1*, Δ*lacZ*::$Spec^R$-P_{tac}-*mKate2*	Fig 4a-c	Chitin biofilm natural transformation assays	Parent (chitin biofilm NT assays)
TND4366 / SAD4059 / (24)	Δ*VC1807*::Cm^R-P_{tac}-*gfp*::*parST1*, Δ*lacZ*::$Spec^R$-P_{tac}-*mKate2*, Δ*pilU*::Tm^R	Fig 4a-c	Chitin biofilm natural transformation assays	Δ*pilU* (chitin biofilm NT assays)
AET254 / SAD4060	Δ*VC1807*::Cm^R-P_{tac}-*gfp*::*parST1*, Δ*lacZ*::$Spec^R$-P_{tac}-*mKate2*, *pilT*^{R35E}	Fig 4a-c	Chitin biofilm natural transformation assays	*pilT*^{R35E} (chitin biofilm NT assays)
TND0428 / SAD2537 / (18)	*comP*^{T129C}	Fig 5b	*A. baylyi* natural transformation assays	Parent (*A. baylyi* NT assays)
TND0799 / SAD2544 / (18)	*comP*^{T129C}, Δ*pilTU*::Zeo^R	Fig 5b	*A. baylyi* natural transformation assays	Δ*pilT* (*A. baylyi* NT assays)
TND0798 / SAD2543 / (18)	*comP*^{T129C}, Δ*pilU*::Zeo^R	Fig 5b	*A. baylyi* natural transformation assays	Δ*pilU* (*A. baylyi* NT assays)
AET392 / SAD4061	*comP*^{T129C}, *pilT*^{D2K,D53R} Δ*pilU*::Zeo^R	Fig 5b	*A. baylyi* natural transformation assays	*pilT*^{D2K,D53R} (*A. baylyi* NT assays)
TND1122 / SAD2540 / (18)	*comP*^{T129C}, *pilT*^{K136A}	Fig 5b	*A. baylyi* natural transformation assays	*pilT*^{WA} (*A. baylyi* NT assays)
TND1135 / SAD2538 / (18)	*comP*^{T129C}, *pilT*^{K136A} Δ*pilU*::Zeo^R	Fig 5b	*A. baylyi* natural transformation assays	*pilT*^{WA}, Δ*pilU* (*A. baylyi* NT assays)
AET316 / SAD4062	*comP*^{T129C}, *pilT*^{D2K,D53R,K136A}	Fig 5b	*A. baylyi* natural transformation assays	*pilT*^{WA,D2K,D53R} (*A. baylyi* NT assays)
AET302 / SAD4063	*comP*^{T129C}, *pilT*^{K136A} *pilU*^{K351D}	Fig 5b	*A. baylyi* natural transformation assays	*pilT*^{WA}, *pilU*^{K351D} (*A. baylyi* NT assays)

AET373 / SAD4064	*comP*^{T129C}, *pilT*^{D2K,D53R,K136A} *pilU*^{K351D}	Fig 5b	*A. baylyi* natural transformation assays	*pilT*^{WA,D2K,D53R}, *pilU*^{K351D} (*A. baylyi* NT assays)
AET399 / SAD4065	E7946 Sm^{R}, P$_{tac}$-*tfoX*, Δ*luxO*, *pilA*^{S67C}, Δ*pilT*::Smx^{R}, Δ*lacZ*::Spec^{R}-P$_{pilT}$-*mCherry*-L5-*pilT*	Fig S2a-b	Fluorescence microscopy foci quantification	*mCherry-pilT*$^{+}$, *pilU*$^{+}$
AET367 / SAD4066	E7946 Sm^{R}, P$_{tac}$-*tfoX*, Δ*luxO*, *pilA*^{S67C}, Δ*pilT*::Smx^{R} *mCherry*-L5-*pilU*, Δ*lacZ*::Spec^{R}-P$_{pilT}$-*pilT*	Fig S2a-b	Fluorescence microscopy foci quantification	*mCherry-pilU*$^{+}$, *pilT*$^{+}$
AET208 / SAD4067	E7946 Sm^{R}, P$_{tac}$-*tfoX*, Δ*luxO*, *pilA*^{S67C}, Δ*pilTU*::Tm^{R}, Δ*lacZ*::Spec^{R}-P$_{pilT}$-*pilT*^{R35E}	Fig S5a-b	Transformation, pilus labeling, and cellular aggregation assays	*pilT*^{R35E}
AET209 / SAD4068	E7946 Sm^{R}, P$_{tac}$-*tfoX*, Δ*luxO*, *pilA*^{S67C}, Δ*pilTU*::Tm^{R}, Δ*lacZ*::Spec^{R}-P$_{pilT}$-*pilT*^{K36E}	Fig S5a-b	Transformation, pilus labeling, and cellular aggregation assays	*pilT*^{K36E}
AET397 / SAD4069	E7946 Sm^{R}, P$_{tac}$-*tfoX*, Δ*luxO*, *pilA*^{S67C}, Δ*pilTU*::Tm^{R}, Δ*lacZ*::Spec^{R}-P$_{pilT}$-*pilT*^{D2K,E53R}	Fig S5a-b	Transformation, pilus labeling, and cellular aggregation assays	*pilT*^{D2K,E53R}

Table S2. Primers used in this study.

SOE deletions		
Primer name	**Sequence (5' to 3')**	**Description**
ABD123	ATTCCGGGGATCCGTCGAC	Antibiotic resistance cassette F
ABD124	TGTAGGCTGGAGCTGCTTC	Antibiotic resistance cassette R
BBC374	TGGCAAAAAGCGAGAGAAGAAG	*ΔluxO* F1
BBC375	gtcgacggatccccggaatCATGAGGACATATTTTGTTTTCTGC	*ΔluxO* R1
BBC376	gaagcagctccagcctacaTAAGCGATGAGAGAATGGATCAAC	*ΔluxO* F2
BBC377	TCACACCCGAATTTCCATCATGC	*ΔluxO* R2
DOG0400	ACTTCTGGCTGAAGGTCAATTTTC	*ΔpilT/U* F1
DOG0401	gtcgacggatccccggaatCATTTAAATTCCTTAATAAAGTCTGGC	*ΔpilT* R1
DOG0402	gaagcagctccagcctacaTAGGTAGGTAAAGACAGATGGAG	*ΔpilT* F2
DOG0403	TCACGTGTTCGGCCAAAATC	*ΔpilT/U* R2
DOG0405	gtcgacggatccccggaatCATCTGTCTTTACCTACCTAAAATGC	*ΔpilU* R1
DOG0406	gaagcagctccagcctacaTAGCGATGGTTACTTTGTGCG	*ΔpilU* F2
DOG0436	AAGCGTTCTGGTTCAATCACC	*ΔMSHA* locus (*ΔVC0399-VC0414*) F1
DOG0434	gtcgacggatccccggaatCATTCTCTACCACTGCTATTTGGTTC	*ΔMSHA* locus (*ΔVC0399-VC0414*) R1
BBC2129	gaagcagctccagcctacaTAATGATTAAGCACTCAATGGATCCAG	*ΔMSHA* locus (*ΔVC0399-VC0414*) F2
BBC2130	TTTTGCATCAGCAAAATCACGC	*ΔMSHA* locus (*ΔVC0399-VC0414*) R2
DOG0575	TATGTGCAAGAGCTCAAAGGC	*ΔpilC* F1
DOG0574	gtcgacggatccccggaatCATGTTGAGGCTCGTGCTG	*ΔpilC* R1
DOG0576	gaagcagctccagcctacaTAGTATGGCGACAAACGGC	*ΔpilC* F2
DOG0577	AACCGCAGTGGTAAAGCTTTG	*ΔpilC* R2
BBC1881	TTTAAAGGGGATCAGTGACCG	*ΔVC1807*::Ab^R F1
ABD340	gtcgacggatccccggaatACGTTTCATTAGTCACCTCTATTGTTAACTTGTTC	*ΔVC1807*::Ab^R R1
ABD341	gaagcagctccagcctacaTAGTCGAAAATAAAAAAAAGAGGCTCGCCTC	*ΔVC1807*::Ab^R F2
BBC1882	CAATTTTGCTTTTGGACCATCCC	*ΔVC1807*::Ab^R R2
ABD725	GAAGCAGCTCCAGCCTACA	Detect F for all deletions (unless another F primer is provided)
BBC1661	GGCTGATTTCTTTCAAATATACCAG	*ΔluxO* detect R

DOG0407	TCATCAAGATAAGCATGAGTCAG	*ΔpilU* detect R
BBC2131	GAAATGAGAAAAGGAAAATTGCAC	*ΔMSHA* detect R
DOG0578	AATCACTAAGCTCATGAGGGC	*ΔpilC* detect R
BBC3918	ggaaaaagacccagtgcgtTCCATGTTGTCGGAATCGC	*ΔpilT* detect F (band if PilT present)
DOG0404	TTCTGCTTGCCTTGCGTC	*ΔpilT* detect R (band if PilT present)
BBC695	gaagcagctccagcctacaGAACAGGTTTAATCATGAATGACG	*ΔpilT* detect constant band F
BBC702	GTGATTGAGTATGGGCTTATGG	*ΔpilT* detect constant band R
BBC1934	GTTACAAAGTCAGGGACGTAAAG	*ΔpilT/U* (A. baylyi) F1
BBC1939	GGTATTCAGATTGATCGTCAGTTAG	*ΔpilT/U* (A. baylyi) R2
BBC1935	gtcgacggatccccggaatATCCATATTTTCCCCGAAGATCG	*ΔpilT* (A. baylyi) R1
BBC1936	gaagcagctccagcctacaTAAGAATAACGCTACTCGATCTG	*ΔpilT* (A. baylyi) F2
BBC1937	gtcgacggatccccggaatCATCGTATTGTTTTCCTCTCAGATC	*ΔpilU* (A. baylyi) R1
BBC1938	gaagcagctccagcctacaCGCCGTAATCTCAAATAAAAGAG	*ΔpilU* (A. baylyi) F2
Fluorescent fusions		
Primer name	**Sequence (5' to 3')**	**Description**
BBC1835	GCaGGTGGAAGTGGTGGAgtgagcaagggcgaggagg	*mCherry*-L5 F
BBC5106	gccagctttcgcggcagcttcgccaccagaaccgctCTTGTACAGCTCGTCCATGCCGCCGGTGGAGTG	*mCherry*-L5 R
BBC3669	ttctggtggcgaagctgccgcgaaagctggcGTGagcaagggcgaggaggataacatgg	L5-*mCherry* F
BBC3223	tccacctgctccacctgccttgtacagctcgtccatgccgccggtggag	L5-*mCherry* R
BBC279	GCaGGTGGAAGTGGTGGACGTAAAGGAGAAGAACTTTTC	*gfp*-L5 F
BBC5105	gccagctttcgcggcagcttcgccaccagaaccgctGTTGTATAGTTCATCCATGCCATG	*gfp*-L5 R
ABD332	GGCTGAACGTGGTTGTCGAAAATGAC	*ΔlacZ*::X-L5-*pilT* F1
ATP0002	tccaccacttccacctgcCATTTAAATTCCTTAATAAAGTCTGGC	X-L5-*pilT* R1
ATP0005	agcggttctggtggcgaagctgccgcgaaagctggcGATATCGCTGAGTTACTGGAAT	X-L5-*pilT* F2
ABD256	CCCAAATACGGCAACTTGGCG	*ΔlacZ*::X-L5-*pilT* R2
BBC4710	AAGACCCAGAACAACAAGCC	X-L5-*pilU* F1
JCP028	tccaccacttccacctgcCATCTGTCTTTACCTACCTAAAATGC	X-L5-*pilU* R1
ATP0015	agcggttctggtggcgaagctgccgcgaaagctggcGAGTTGAATCAATATCTGGATGGC	X-L5-*pilU* F2
DOG0403	TCACGTGTTCGGCCAAAATC	X-L5-*pilU*
ABD332	GGCTGAACGTGGTTGTCGAAAATGAC	*ΔlacZ*::*pilT*-L5-X F1

ATP0006	gccagctttcgcggcagcttcgccaccagaaccgctAAATGCTTTTAAATCCAACTCGAT	*pilT*-L5-X R1
ATP0007	gcaggtggagcaggtggaTAGGTAGGTAAAGACAGATGGAGTTGA	*pilT*-L5-X F2
ABD256	CCCAAATACGGCAACTTGGCG	*ΔlacZ*::*pilT*-L5-X R2
ATP0083	agcggttctggtggcgaagctgccgcgaaagctggcGccATCGCTGAGTTACTGGAAT	X-L5-*pilT* D2A F2
BBC1839	gcatggacgagctgtacaag	*mCherry* detect F
BBC4021	caggatgtcccaggcgaa	*mCherry* detect R
BBC1903	tcgaaagatcccaacgaaaag	*gfp* detect F
BBC3897	CAAGCGATGTACATCAGAATGGG	X-*pilT* detect R
DOG0404	TTCTGCTTGCCTTGCGTC	X-*pilU* detect R
JCP314	GCAATTCGGAACTTGATCCGTG	*pilT*-X detect F
Point mutations		
Primer name	**Sequence (5' to 3')**	**Description**
BBC401	ACCAGCAAAGCTAATAAAATCGAG	*pilA* F
BBC404	CGCCATACTAACCCAATACACTC	*pilA* R
DOG0400	ACTTCTGGCTGAAGGTCAATTTTC	*pilTU* F
DOG0403	TCACGTGTTCGGCCAAAATC	*pilTU* R
ABD332	GGCTGAACGTGGTTGTCGAAAATGAC	*lacZ* F
ABD256	CCCAAATACGGCAACTTGGCG	*lacZ* R
HQP0002	CGCCAAGGTCGTCGAagcACCCGAGCCC	$pilT^{K136A}$ R1
HQP0001	GGGCTCGGGTgctTCGACGACCTTGGCG	$pilT^{K136A}$ F2
BBC2369	GGCTGCCATAGTGGTCGAggcACCCGAACCGGTTGCGC	$pilU^{K134A}$ R1
BBC2370	GCGCAACCGGTTCGGGTgccTCGACCACTATGGCAGCC	$pilU^{K134A}$ F2
BBC5056	CTTCTAATTTggCagCATATTCACTGCGCTGGGCATCATTCATGAT	$pilT^{E64A,E65A}$ R1
BBC5057	AGTGAATATGctGccAAATTAGAAGTCGATTTTTCTTTTGAACTGC	$pilT^{E64A,E65A}$ F2
BBC5059	GCACGCCAAGggcagcAACTTCGCCATCAATCCGTACCATAGGCGG	$pilT^{R35A,K36A}$ R1
BBC5060	TGGCGAAGTTgctgccCTTGGCGTGCCTGCTTTTACCCATTCTGAT	$pilT^{R35A,K36A}$ F2
ATP0076	AGTAACTCAGCGATggCCATTTAAATTCCTTAATAAAGTCTGGCTATGCGTAG	$pilT^{D2A}$ R1
ATP0075	AGGAATTTAAATGGccATCGCTGAGTTACTGGAATTTAGTGTAAAACATAACGC	$pilT^{D2A}$ F2
ATP0079	GCATCATTCATGATagCAAAAATCAAGCGATGTACATCAGAATGGGTAAAAGC	$pilT^{E53A}$ R1
ATP0078	TCGCTTGATTTTTGctATCATGAATGATGCCCAGCGCAGTGAATATGAA	$pilT^{E53A}$ F2
ATP0019	CGCCAAGCTTttcAACTTCGCCATCAATCCGTACCATAGGCGGAAC	$pilT^{R35E}$ R1
ATP0018	TGGCGAAGTTgaaAAGCTTGGCGTGCCTGCTTTTACCCATTCTGAT	$pilT^{R35E}$ F2
BBC5181	ACCATCGCTAtTtCATtTtAATCTTCACATTCTGCAAAGAGCCGC	$pilU^{D366K,E368K}$ R1
BBC5182	AAGATTaAaATGaAaTAGCGATGGTTACTTTGTGCGCTTTGC	$pilU^{D366K,E368K}$ F2
ATP0022	GCACGCCAAGtTcCCTAACTTCGCCATCAATCCGTACCATAGGCGG	$pilT^{K36E}$ R1
ATP0021	CGAAGTTAGGgAaCTTGGCGTGCCTGCTTTTACCCATTCTGATGTA	$pilT^{K36E}$ F2

ATP0025	ATCGCTACTCCATtTtAATCTTCACATTCTGCAAAGAGCCGCTGCCGTA	*pilU*^{D366K} R1
ATP0024	GAATGTGAAGATTaAaATGGAGTAGCGATGGTTACTTTGTGCGCTTTGC	*pilU*^{D366K} F2
ATP0028	AGTAACCATCGCTAtTtCATATCAATCTTCACATTCTGCAAAGAGC	*pilU*^{E368K} R1
ATP0027	TGAAGATTGATATGaAaTAGCGATGGTTACTTTGTGCGCTTTGCTT	*pilU*^{E368K} F2
ATP0046	AGTAACTCAGCGATtTtCATTTAAATTCCTTAATAAAGTCTGGCTATGCGTAG	*pilT*^{D2K} R1
ATP0045	AGGAATTTAAATGaAaATCGCTGAGTTACTGGAATTTAGTGTAAAACATAACGC	*pilT*^{D2K} F2
ATP0064	GCATCATTCATGATgcgAAAAATCAAGCGATGTACATCAGAATGGGTAAAAGC	*pilT*^{E53R} R1
ATP0063	TCGCTTGATTTTTcgcATCATGAATGATGCCCAGCGCAGTGAATATGAA	*pilT*^{E53R} F2
ATP0073	CACGCTTGGTaTcGAGCATCAAACGCAGATCGTTGGCTGAATCGGC	*pilU*^{K348D} R1
ATP0072	TTTGATGCTCgAtACCAAGCGTGGTGATGACTACGGCAGCGGCTCT	*pilU*^{K348D} F2
DOG0175	AAACTATCCAGATAAGGGAAAGC	*comP* (A. baylyi) F
DOG0178	AGGATCTGTAATGACGGGTTGAG	*comP* (A. baylyi) R
CE87	GAAGTTGTCGTACATTTCCAACATACAGCGCCACTAGCATATG	*comP*^{T129C} (A. baylyi) R1
CE88	CATATGCTAGTGGCGCTGTATGTTGGAAATGTACGACAACTTC	*comP*^{T129C} (A.baylyi) F2
BBC1934	GTTACAAAGTCAGGGACGTAAAG	*pilT/U* F (A. baylyi)
BBC1939	GGTATTCAGATTGATCGTCAGTTAG	*pilT/U* R (A. baylyi)
BBC2403	GCTGCAAGGGTGGTTGAagcACCGGAACCAGTGG	*pilT*^{K136A} R1 (A. baylyi)
BBC2404	CCACTGGTTCCGGTgctTCAACCACCCTTGCAGC	*pilT*^{K136A} F2 (A. baylyi)
ATP0096	CGAGTAATTCTGTTATtTtCATATTTTCCCCGAAGATCGTCAAAAGGTTTAATTATTTTG	*pilT*^{D2K} R1 (A. baylyi)
ATP0092	CGGGGAAAATATGcgTATAACAGAATTACTCGCGTTTTCGGTGC	*pilT*^{D2K} F2 (A. baylyi)
ATP0099	GTTTATCATTCATAATAcgGTAAATGAGATTATGGACTTCTGAATGATCCATTGCAG	*pilT*^{D53R} R1 (A. baylyi)
ATP0100	GTCCATAATCTCATTTACcgTATTATGAATGATAAACAGCGCCGAGACTACGAAG	*pilT*^{D53R} F2 (A. baylyi)
ATP0109	TCTTCCGAAAGaTcGATCTGTAGACGTAAATTATTAGGCGAGTCTGC	*pilU*^{K351D} R1 (A. baylyi)
ATP0110	GTCTACAGATCgAtCTTTCGGAAGAAGCCAACAAACCCCTAG	*pilU*^{K351D} F2 (A. baylyi)
HQP0004	GCGCAGTGAATATGAAGAG	*pilT*^{K136A} detect F
HQP0003	GCCAAGGTCGTCGGagc	*pilT*^{K136A} detect R
BBC2372	ATTTTGTATCGAGTCGATGGTG	*pilU*^{K134A} detect F
BBC2371	GCCATAGTGGTCGgggc	*pilU*^{K134A} detect R
BBC2386	tcactgcccgctttccagtcCTCAAGAATTGCCTCGACG	*pilT*^{E64A,E65A} detect F
BBC5058	AATCGACTTCTAATTTggtag	*pilT*^{E64A,E65A} detect R
BBC5061	TGATGGCGAAGTcgctgcc	*pilT*^{R35A,K36A} detect F

HQP0002	CGCCAAGGTCGTCGAagcACCCGAGCCC	*pilT*^{R35A,K36A} detect R
ATP0077	CAGACTTTATTAAGGAATTTAAATGacc	*pilT*^{D2A} detect F
ATP0080	GATGTACATCGCTTGATTTTTact	*pilT*^{E53A} detect F
ATP0020	ATTGATGGCGAAGTcgaa	*pilT*^{R35E} detect F
BBC5183	GCAGAATGTGAAGATTaAaATGaga	*pilU*^{D366K,E368K} detect F
ATP0023	GATGGCGAAGTTAGGgga	*pilT*^{K36E} detect F
ATP0026	TGCAGAATGTGAAGATTaga	*pilU*^{D366K} detect F
ATP0029	AGAATGTGAAGATTGATATGaga	*pilU*^{E368K} detect F
ATP0047	CAGACTTTATTAAGGAATTTAAATGaga	*pilT*^{D2K} detect F
ATP0065	GATGTACATCGCTTGATTTTccgc	*pilT*^{E53R} detect F
ATP0074	CTGCGTTTGATGCTCggt	*pilU*^{K348D} detect F
HQP0158	gtcgacggatccccggaatctaAATTTTGCTGAAGATTTCAGGAGC	*pilT* mutation detect R
DOG0407	TCATCAAGATAAGCATGAGTCAG	*pilU* mutation detect R
BBC2406	CAATGGATCATTCAGAAGTCC	*pilT*^{K136A} (A. baylyi) detect F
BBC2405	TGCAAGGGTGGTTGgagc	*pilT*^{K136A} (A. baylyi) detect R
CE89	TGCTAGTGGCGCTGTATGT	*comP*^{T129C} (A.baylyi) detect F
CE59	GCAATTAGCTCTTTATATAAAGTAG	*comP*^{T129C} (A.baylyi) detect R
ATP0095	GCTGCCCAAGTTGATACATC	*pilT*^{D2K} (A. baylyi) detect F
ATP0098	AACGCGAGTAATTCTGTTATtct	*pilT*^{D2K} (A. baylyi) detect R
DOG1040	ATTGACAGGGTTCTCATTTCAA	*pilT*^{D53R} (A. baylyi) detect F
ATP0101	CGCTGTTTATCATTCATAATgcg	*pilT*^{D53R} (A. baylyi) detect R
ATP0107	TACATGCCAATAATGCCAATC	*pilU*^{K351D} (A. baylyi) detect F
ATP0108	GGCTTCTTCCGAAAGtcc	*pilU*^{K351D} (A. baylyi) detect R

Movie S1. Molecular dynamics simulation of the AF3 PilT-PilU model. A 100-ns span of the simulation is show for $PilT^{R35}$-$PilU^{D366,E368}$.

Movie S2. Molecular dynamics simulation of the AF3 PilT-PilU model. A 100-ns span of the simulation is show for $PilT^{R35}$-$PilU^{I365,M367}$.

Movie S3. Molecular dynamics simulation of the AF3 PilT-PilU model. A 100-ns span of the simulation is show for $PilT^{K36}$-$PilU^{D366,E368}$.

Movie S4. Molecular dynamics simulation of the AF3 PilT-PilU model. A 100-ns span of the simulation is show for $PilT^{D2,E53}$-$PilU^{K348}$.

Dataset S1. Summary statistics for all quantitative data in the manuscript.